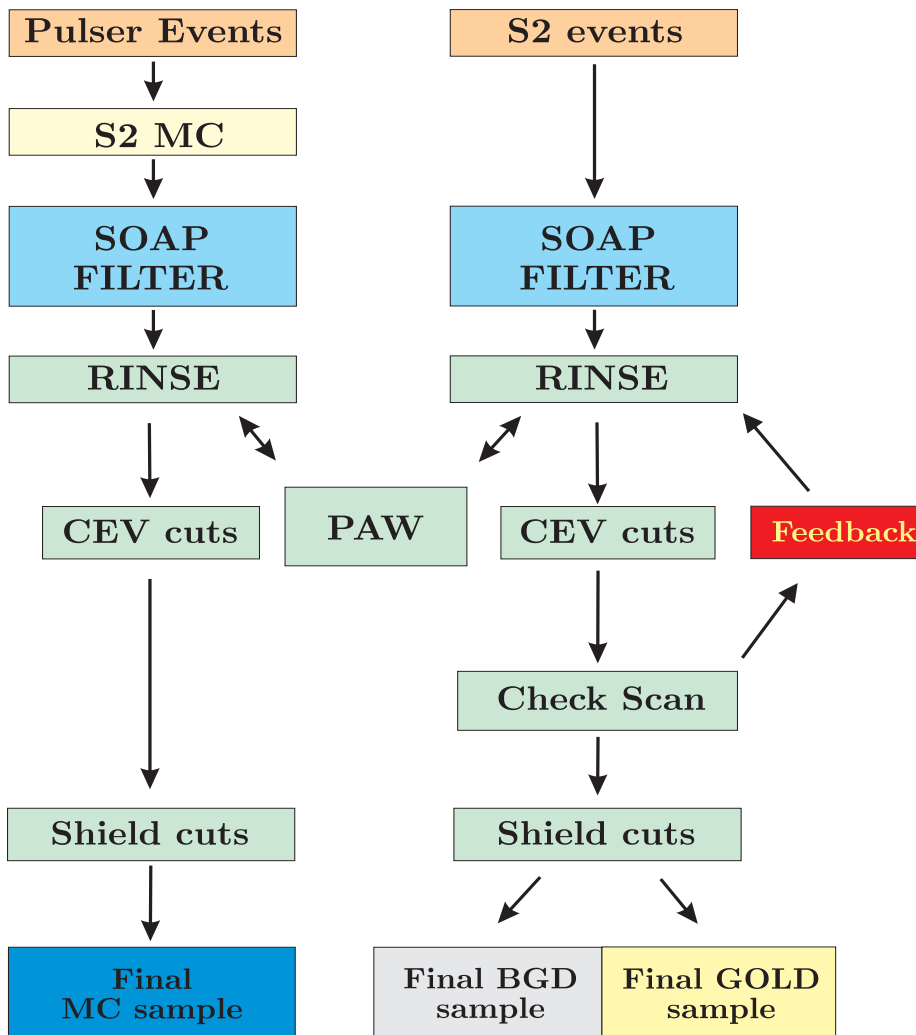


## 5. Event Selection

This chapter deals with the first step in the data analysis: the event selection. Out of the  $\sim 10^7$  triggers the Soudan 2 detector records every year, only some 100 events will end up in the final contained event sample, often referred to as the **GOLD** event sample. This task is partly undertaken by the standard Soudan 2 **FILTER**, reducing the number of data events by a factor of  $10^3$ . **FILTER** is a conservative piece of software, in that it performs a series of loose cuts, mainly concerned with the trigger and the fiducial volume. Following **FILTER**, a process called **RINSE** (Rapid Isolation of Neutrino Soudan 2 Events) has been developed in Oxford in order to get down to the desirable **GOLD** sample [78]. Event selection with the minimum possible human intervention is achieved by a series of cuts, to be defined shortly. The **RINSE** cuts have been developed (i) by maximising the acceptance of the atmospheric neutrino Monte Carlo simulated data and (ii) by minimising the acceptance of background, which is defined by the event sample that is rejected by the shield (see §5.3.7). The real data acceptance is not taken into account. The cuts may then be fine-tuned (or even re-defined) for optimum performance. Such multiple iterations of event selection are possible because of the short time-scale involved – typically one week for a year’s worth of data once the whole mechanism has been set up. A schematic overview of the event reduction process is shown in fig. 5.1.

Both **MC** and real data are processed with the latest version of **SOAP** before being fed into **RINSE**. **RINSE** processes the events that have been selected by **FILTER**. These events are stored in the so-called **CE3** tapes. **FILTER** has been developing over the years and the latest version (release 23) is more efficient in background rejection than the earlier versions which created the **CE3** tapes at the time of data acquisition. For this reason, **FILTER23** has been run on all **CE3** events before passing them to **RINSE**. This removes biases between



• **Figure 5.1:** Schematic overview of the event selection process. RINSE allows for feedback and rapid re-analysis of the whole sample.

DATA and MC, because the latter has only been processed with release 23 SOAP. It is assumed here that the Contained Event (CEV) acceptance of release 23 is the same as that of earlier SOAP versions. This is believed to be the case because the standard SOAP and FILTER event-rejection algorithms are very loose and reject events which are unambiguously outside the detector's fiducial volume (see the fiducial volume cut, §5.3.2).

The Soudan 2 data analysed in the present thesis has been collected between 26<sup>th</sup> August 1991 and 22<sup>nd</sup> December 1996, a period that corresponds to run range 30000 to 74999 (Table 5.1). A MC sample of 115.7 times the experiment's exposure has been

DATA Attributes		
Number of CE3 Events Processed		35853
DATA Exposure (kTon-Years)	Total	3.341
	Fiducial	2.679
MCNO Attributes		
MCNO Interactions Generated		149014
kTon-Years Generated (at 385 events / kTon-Year)		386.5
Ratio of Exposures MCNO/DATA		115.7

• **Table 5.1:** Number of events and exposures for **DATA** and **MCNO** samples analysed for run range 30000-74999.

generated, in order to provide a large, simulated sample of atmospheric neutrino interactions in the detector. The **MC** events were superposed on **PULSER** data collected over that period (see §4.2.1).

## 5.1 Event Samples: Definitions

The data sets used in this analysis are conveniently labelled. There are two **MC** samples, **MCAF** (**MC All Flavours**) and **MCNO** (**MC No Oscillations**), described in §4.3. The **DATA** sample is divided into the **GOLD** and **BGD** samples after the application of the shield cuts.

- **The GOLD Event Sample**

The **GOLD** neutrino sample consists of the set of events which are fully contained in the detector. Also these events have no associated shield activity, which would otherwise point to possible external particles inducing the event.

- **The BGD Event Sample**

The **BGD** event sample is used in the description of the background contamination of **GOLD**. Two sources of background have been identified:

- Cosmic ray muons interact in the rock surrounding the detector and produce showers of particles. Of these, neutral particles (photons, neutrons, etc) may pass through the shield and the outer layers of the main detector and produce a CEV unnoticed. Such events would be prime candidates for background to neutrino interactions in Soudan 2. However, their occurrence is not so frequent. Most of the time charged particles, also produced by the CR-muon, will leave a trace in the shield, vetoing the event. However, a small number of these events will be accepted in the final CEV sample because of shield inefficiency.
- Charged particles, such as CR-muons, may cross the veto shield without leaving a trace because of shield inefficiency. Some of them may not leave a trace in the outer main-detector layers and be accepted by the containment cuts. This will occur very rarely and the contamination of **GOLD** by such events is expected to be very small.

In the analysis that follows the background processes described above are put in one basket. No attempt will be made to identify the contamination of **GOLD** by each of these processes separately.

There is no simulation for the **BGD** sample. This would be a very complex task in itself and only approximate studies have seen the light of day. It would require tracking cosmic ray showers through the rock down to the detector hall and then ask for neutral particles entering the main detector without associated charged particles hitting the veto shield. Also, the processes that contaminate the **GOLD** sample are rare – not more than one third of the 280 events in the final **GOLD** sample are attributed to background (§5.5) – and the simulation would be very sensitive to assumptions.

The alternative used here is to extract a **BGD** sample from the data: the **BGD** sample is therefore defined as the set of fully contained events that have associated shield activity and fail the veto shield cuts.

- **RINSE Development Event Samples**

In the presentation of the RINSE cuts that follows, the data is divided into events that pass or fail the shield cuts. After applying the containment cuts, these event samples will reduce to the final **GOLD** and **BGD** samples. However, in the definition of each cut, one is interested in the nature of the contained event sample *before* this cut has been applied. This introduces the RINSE *development samples*: for each of the automated cuts presented in this chapter, the development **BGD\***, **MCNO\*** (and occasionally) **GOLD\*** samples will be used. These are defined as the final **BGD**, **MCNO** and **GOLD** samples, before the check-scan has been applied, with the events that are rejected by that particular cut added on top. By definition, the development samples are different for each cut.

The development samples will be used to demonstrate the power of each cut alone when all other RINSE cuts have already been applied.

## 5.2 Survey of Cuts

RINSE cuts are divided into two main groups: the containment cuts and the shield cuts.

### 5.2.1 Containment Cuts

The cuts in this section deal with the containment of the event in the main calorimeter detector. The RINSE containment cuts can be grouped into five basic categories. The order the cuts are applied is not important.

- **Error Cuts**

The error cuts deal with software processor *failures* which, in turn, can be due to hardware failures. Their effect on the acceptance is small.

- **Fiducial Volume Cuts**

Charged particles coming into the detector will deposit ionisation in its outer layers. Moreover, many incoming photons will materialise within 20 cm, approximately

corresponding to a radiation length in the Soudan 2 detector. For this reason, events with associated activity in the first 20 cm inside the detector's faces will be rejected from the contained event sample. Most such events have already been rejected by FILTER.

- **Crack Cuts**

Because of the detector's modular design, inter-modular gaps, or *cracks*, typically 10 cm wide, exist between the main detector's modules. Energetic CR-muons reaching the experimental cavity can travel through these cracks to appear inside the detector's fiducial volume. Such events start on a module boundary and can be thus rejected.

- **Data Quality Cuts**

The data quality checks are concerned with the poor performance of software processors, in particular of pulse matching by PMT under hard and not-common situations, such as vertical events etc. Quality cuts are also concerned with CR-muons that have passed all other containment cuts because of a topology very specific to the Soudan 2 calorimeter design. Finally, a group of quality cuts deals with breakdowns and other noise events, typically due to high voltage trips.

- **The Check-Scan**

The data passing all the containment automated cuts is check-scanned by two physicists in the form of a blind mixture of **GOLD** and **BGD** events. The purpose of the procedure is two-fold: (i) to reject the obvious failures of the cuts, i.e. events which are clearly not contained, such as CR-muons and breakdowns; (ii) to evaluate, during the development stage, the performance of the cuts – on the **BGD** and **MCNO** samples only - and, maybe, fine-tune them or re-define them.

## 5.2.2 The Shield Cuts

Associated shield activity will determine whether an event contained by all other cuts will be classified as **GOLD** or **BGD**. In order to remain unbiased in the selection of **GOLD**, the shield

information is considered only after the decision on the containment of the event has been made.

### 5.3 Analysis and Determination of each cut

The data cuts are described and justified below. An event is *rejected* by a cut when it is excluded from the contained event sample. As one might expect, the sets of events rejected by each cut are not mutually exclusive. For this reason, the development of the cuts is an iterative process; one returns to the drawing board many times, especially after acquiring a feeling on the performance of the algorithms after the check-scan, the latter being the last in the series of containment cuts.

In the following sections, each cut is presented by assuming and applying all other RINSE cuts first (excluding the check-scan); this procedure will produce a “clean” event sample on which the effect of the cut is maximised and is thus more easily grasped. Furthermore, the shield cuts will be applied first, which will ease further the demonstration of the logic of each cut. For example, cuts aimed at rejecting cosmic ray muons entering the detector will be developed by comparing **BGD\*** with the **MCNO\*** expectation. On the other hand, breakdown events are not correlated with shield activity; noise and breakdown cuts will be investigated by analysing the **GOLD\*** sample.

#### 5.3.1 The Error Cuts

Three error cuts are in use. These aim to reject events where the detector trigger or software processors failed to function correctly. The **MCNO** sample is used here: it has been generated on top of **PULSER** data (§4.2.1) and the random occurrence of such failures is properly described.

- **Cut0; Event Processed Successfully**

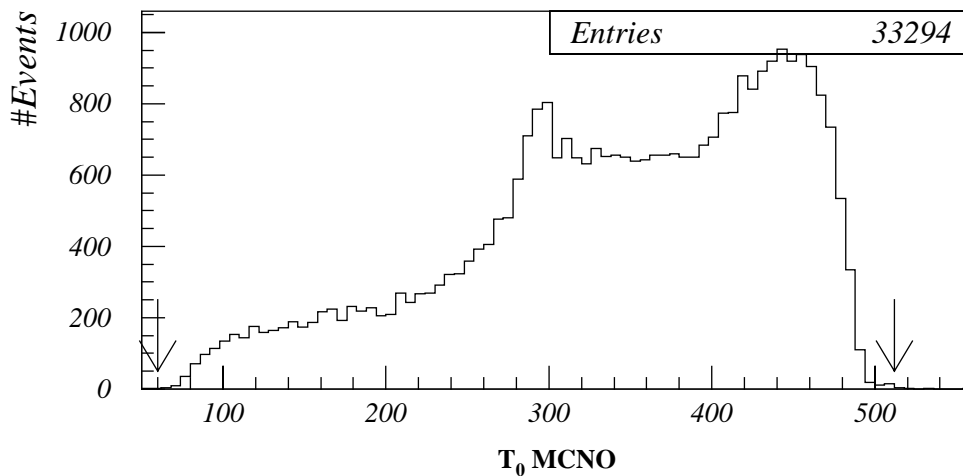
All the processors in the event need to have run successfully. As part of this condition, the event box needs to have at least 6 reconstructed 3D hits. Hit clusters of less than 6 3D hits are very often due to detector noise and are not considered. Moreover, features of the trigger which are understood but are hard to simulate will result in different acceptances between **GOLD** and **MCNO** event samples at this very low end of the energy spectrum.

Let it be noted that, further down the cuts chain, a minimum number of 10 hits in the event box is required in order to reject the vast majority of the breakdown contamination of the **GOLD\*** sample.

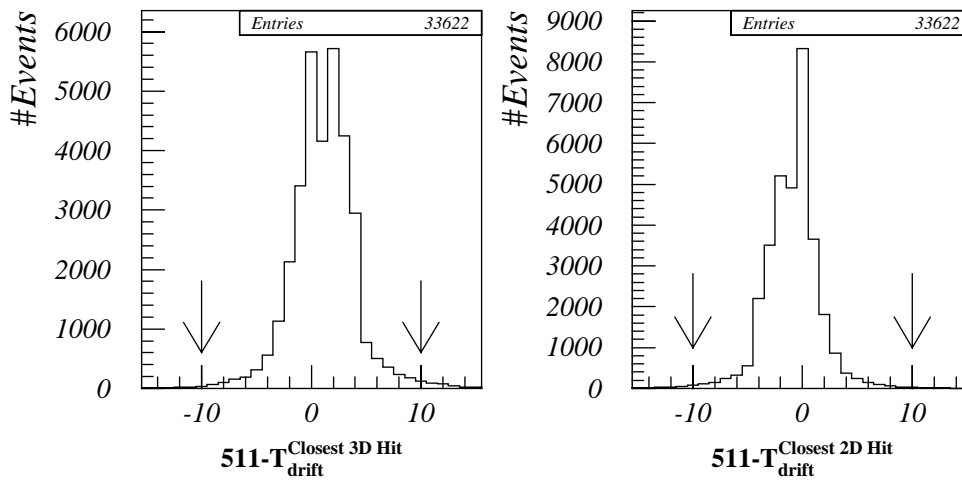
*Cut0* is special: an event that fails will not be processed any further and none of the other RINSE cuts will be defined.

- **CutE1; Physical  $T_0$**

The value of  $T_0$  must be physical, i.e. lie in the range of 60 to 512 dtu (fig. 5.2). An erroneous value of  $T_0$  can occur from random hits in the event box or bad hit reconstruction (§3.3.3). This cut, however, particularly aims at rejecting the rare cases where two events happen within the trigger window. Such a case may occur when the detector triggers on



• **Figure 5.2:** *CutE1*. Distribution of  $T_0$  for MCNO\* events passing all other RINSE cuts. The tails of the distribution below 60 dtu and beyond 512 dtu will be rejected.



• **Figure 5.3: *CutE2*.** The hit with time nearest to the trigger time, 511, is found. The difference  $511 - T_{\text{drift}}$  is plotted. This is done for both reconstructed 3D-hits (left) and clustered 2D hits that can be projected in the event box (right) in each event of the MCNO\* sample after all other RINSE cuts have been applied.

something small and a cosmic ray muon appears in the frame slightly early or late. Since the trigger is not due to the CR-muon, but  $T_0$  is determined by the latter because of its dominant size,  $T_0$  is expected to acquire unphysical values.

#### • **CutE2; Removal of Random Triggers**

The event box must contain at least one of the hits that triggered the event, removing random triggers and rare situations in which the box clustering algorithm has settled on the wrong group of hits. Since the trigger (see §3.1.2) only sees multiplexed 2D hits, the requirement is that *either* a reconstructed 3D hit *or* a clustered 2D hit which can be projected into the event box must lie in the time window of  $511 \pm 10$  dtu (fig. 5.3).

### 5.3.2 The Fiducial Volume Cut

In order to obtain a pure neutrino sample, it is necessary to exclude all particles incoming to the main detector, be they cosmic ray muons or products of particle interactions in the rock surrounding the detector cavity. This is partly achieved by rejecting all events which have

associated activity in the outer layers of the main calorimeter. The detector volume within which events are contained is called the *fiducial volume*. The standard Soudan 2 FILTER applies a fiducial volume cut: an event is rejected if it has a SEARCH track with three or more 2D hits within 20 cm of the outside. The distance of 20 cm has been chosen because the radiation length in the Soudan 2 main calorimeter is  $\approx 15$  cm; most of the electromagnetic radiation will have interacted before entering the detector's fiducial volume. Moreover, only a small fraction of charged particles travelling 20 cm through a calorimeter module will not leave a trace and enter the fiducial volume unnoticed.

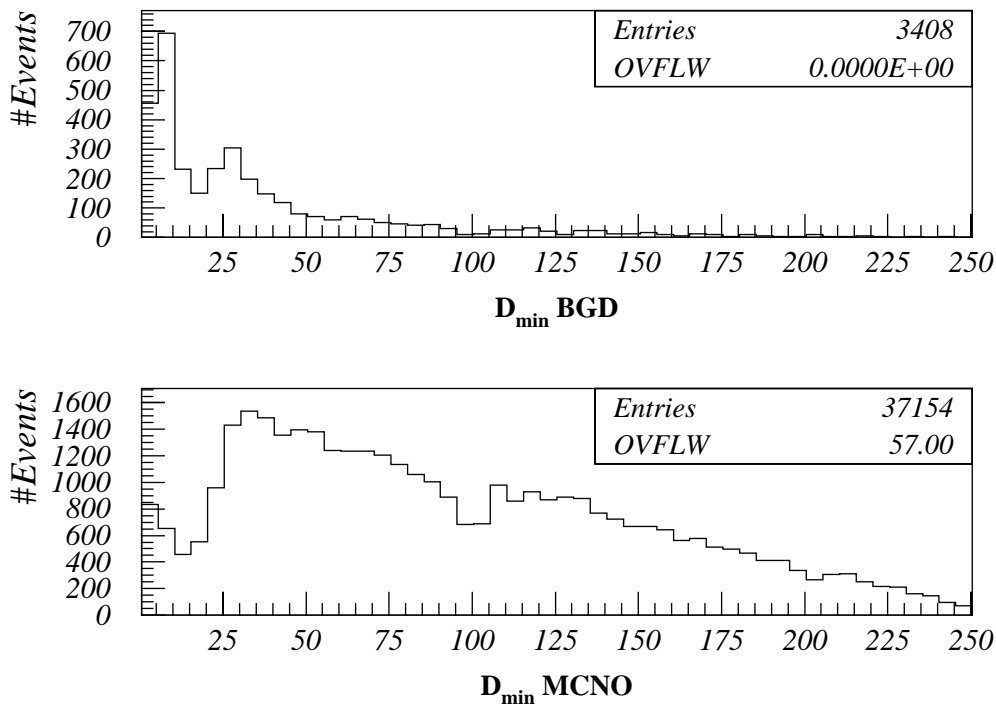
- **CutFV; Fiducial Volume Cut**

The performance of processor FILTER in rejecting incoming charged particles is evaluated by the depth distribution of the event. The depth estimator,  $D_{\min}$ , is defined as the shortest distance to the detector *skin* from any of the six sides of the event box.<sup>9</sup> A significant amount of BGD\* remains below  $D_{\min}$  of 25 cm, which corresponds to approximately 20 cm of active detector (fig. 5.4). These events are rejected.

The RINSE fiducial volume cut of 20 cm from any of the six faces of the Soudan 2 detector is applied to the hits in the event box. The distance of 20 cm of active detector corresponds to the spacing of 13 anode cables or 20 cathode strips. Therefore, an event is rejected if a hit in the event box lies on anodes 1-13 or 242-255, if the latter are external to the detector (as in an L-shaped main calorimeter configuration), or if it lies on cathodes 1-20 or 475-495. The above only covers the top-bottom and east-west detector faces. For the end-looms of the north and south detector faces an event is rejected if  $D_{\min} - (T_0^{\max} - T_0) \times V_d < 25$  cm, where  $V_d$  is the module drift speed in cm/dtu; this takes into account how much the event can be stretched along the drift (z) axis, which is determined by the magnitude of  $T_0^{\max} - T_0$ . In this fashion end-loom events will be kept only if they have a narrow  $T_0$ -window that restricts them within the fiducial volume.

---

<sup>9</sup> In the scanned analysis the depth of an event is defined as the shortest distance between the reconstructed vertex to the outside of the detector, where the bottom face is not considered.

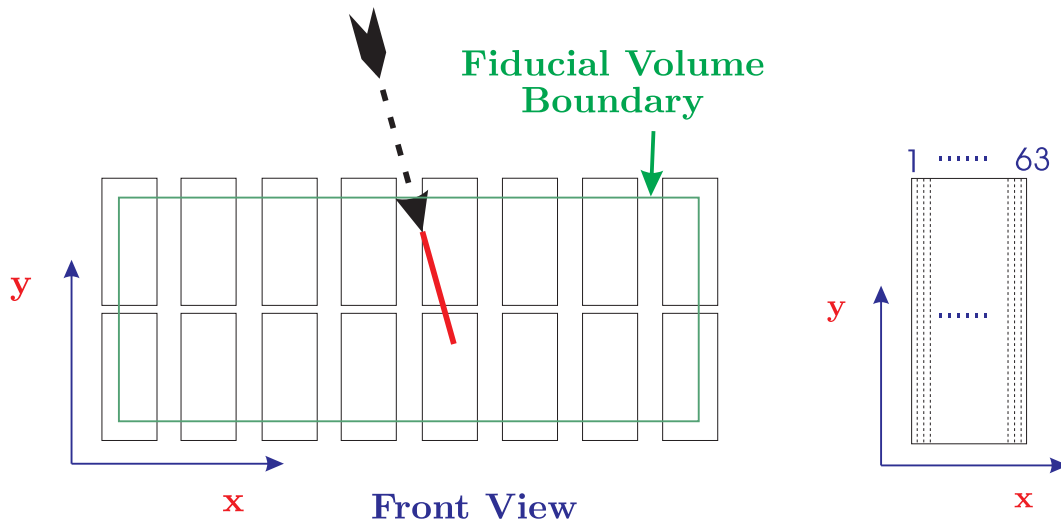


• **Figure 5.4:** *CutFV*. Distribution of  $D_{\min}$ , shortest distance to the outside of the detector from any of the 6 faces of the event box; **BGD\*** (top) and **MCNO\*** (bottom) samples passing all other RINSE cuts.

Finally, note that the RINSE fiducial volume cut is harsher than the FILTER cut because it will reject any event with at least one 3D hit in the outer 20 cm of active detector.

### 5.3.3 The Crack Cuts

The crack cuts are designed to reject the CR-muons entering the calorimeter detector through inter-modular gaps (fig. 5.5). This is a very important cut and is simple in its implementation. Because of the rock overburden, CR-muons reach the detector always from above. We therefore look at the top of the event and examine the distributions of  $A^{\text{Top}}$ , the anode channel, or  $C^{\text{Top}}$ , the cathode channel, or  $T_{\text{drift}}^{\text{Top}}$ , the time, of the highest hit in the event box and ask whether there is any abundance of events near the module edges. For the vertical (anode and wireplane) cracks, the angle between the event axis (§3.3.4) and the

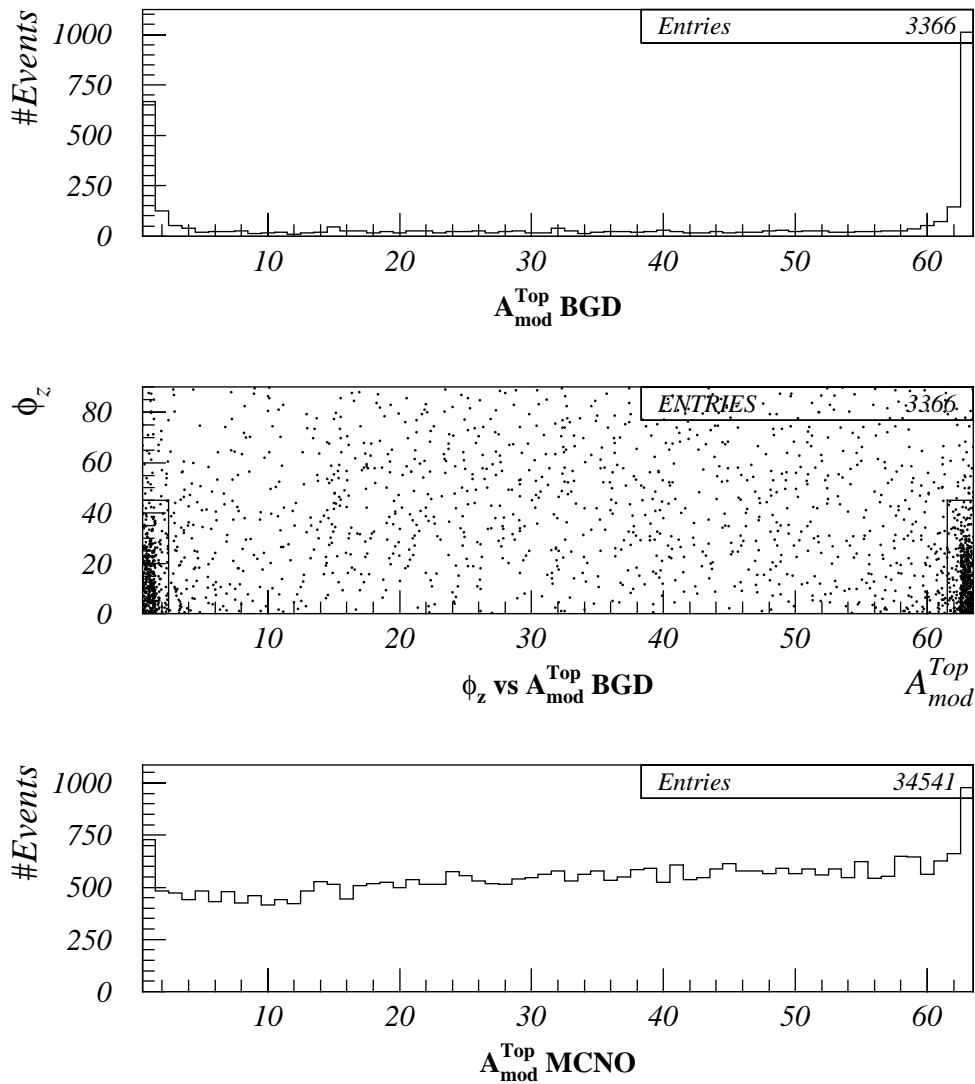


• **Figure 5.5:** Graphical illustration of a cosmic ray muon entering the detector through an anode crack, which is parallel to the  $y$ - $z$  detector plane. The muon may appear within the fiducial volume but can be rejected because it starts on a module boundary. In this particular case, the muon is expected to start on anode channels 1 or 63 of the module, as seen on the right. Cosmic ray muons entering the main detector through the wireplane ( $y$ - $x$ ) or cathode ( $x$ - $z$ ) cracks can similarly be rejected. The size of the cracks has been exaggerated.

plane of the crack is also of interest, since it is expected to be small for muons propagating down the crack before they enter the detector.

- **CrX; Anode Crack Cut**

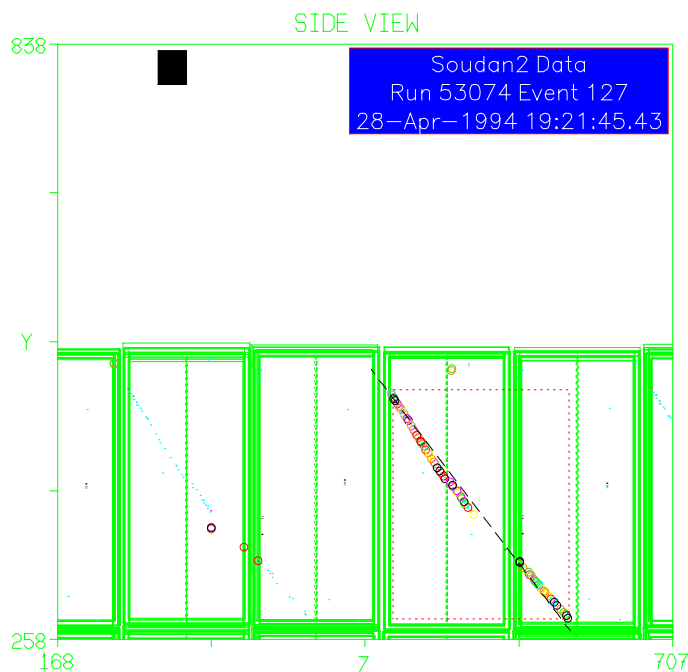
The distribution for the **BGD\*** sample of  $A_{\text{mod}}^{\text{Top}}$ , the anode cable in module space (ranging between 1 and 63) of the highest hit in the event box, clearly shows an excess in the edge anode wires 1 and 63 (fig. 5.6). Moreover, for  $\phi_z > 45^\circ$ , where  $\phi_z$  is the angle between the event axis and the  $y$ - $z$  plane of the anode crack, the population at the edge anode wires is consistent with no CR-muon excess. The **MCNO\*** distribution of  $A_{\text{mod}}^{\text{Top}}$  is nicely flat; the increased population at the edge anode wires is due to the skin of the modules, which absorbs energy but is not instrumented. On the basis of these plots, events with their highest hit on anodes 1, 2, 62 or 63 and with  $\phi_z < 45^\circ$  are rejected. The acceptance is reduced by 55.3% for **BGD\*** and by 3.7% for **MCNO\*** when all other RINSE cuts have previously been applied.



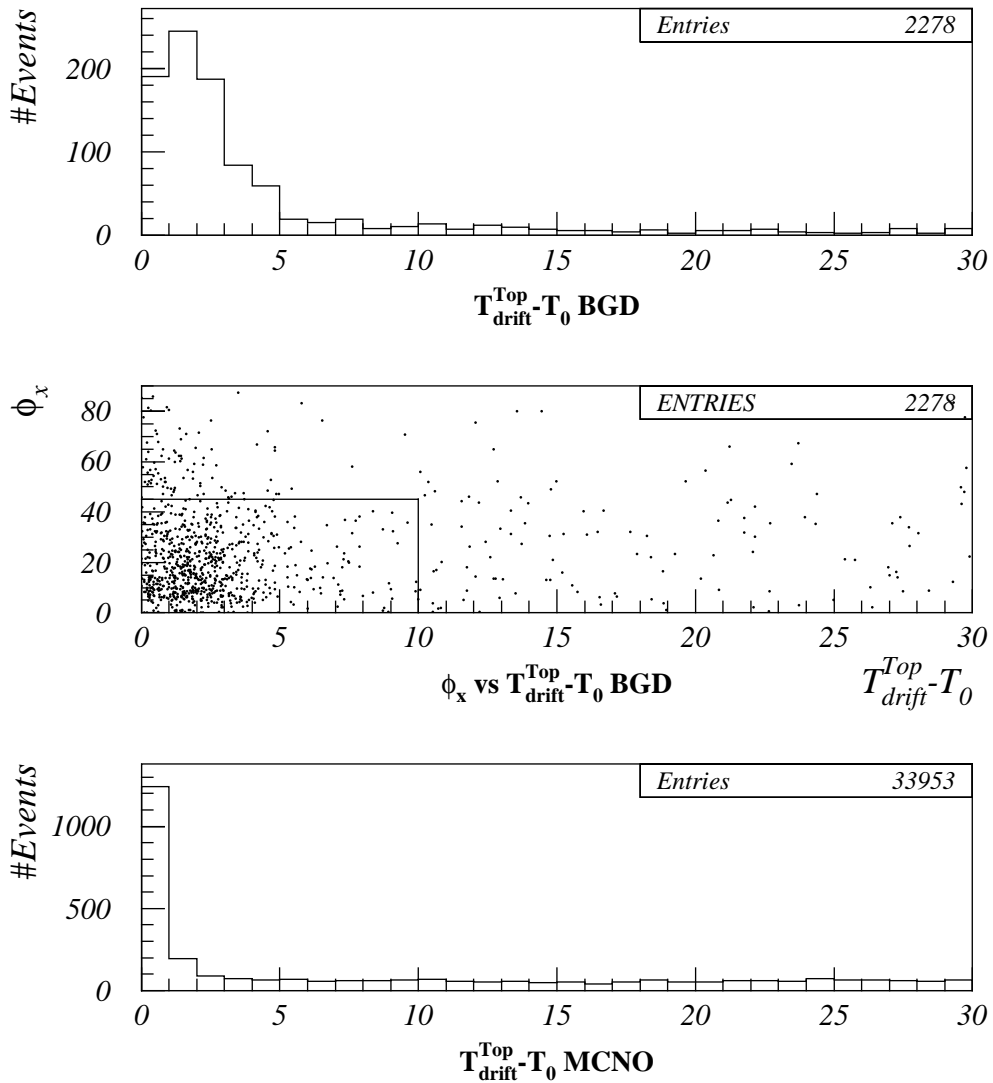
• **Figure 5.6:** *CrX*. Distribution of  $A_{\text{mod}}^{\text{Top}}$ , the anode channel in module space of the highest hit in the event box, for **BGD\*** (top); distribution of  $\phi_z$ , the angle between event axis and plane of anode crack, versus  $A_{\text{mod}}^{\text{Top}}$  for **BGD\*** (middle); distribution of  $A_{\text{mod}}^{\text{Top}}$  for **MCNO\*** (bottom). All other RINSE cuts have already been applied in all three plots. The boxes on the scatter plot show where the cut is placed. The different populations of channels 1 and 63 in the top plot are due to the fact that anode 1 is at the outside the fiducial volume for the outer of the four modules in a loom. Hence, channel 1 is expected to carry  $\frac{3}{4}$  the events channel 63 does.

- **CrZ; Wireplane Crack Cut**

An example of a CR-muon entering the main detector through the wireplane is given in fig. 5.7. By definition, a hit will be on the wireplane if its time is equal to  $T_0$ . The **BGD\*** distribution of  $T_{\text{drift}}^{\text{Top}} - T_0$ , where  $T_{\text{drift}}^{\text{Top}}$  is the time of the highest hit in the event box, exhibits a very clear peak towards zero (fig 5.8). For  $\phi_x > 45^\circ$ , where  $\phi_x$  is the angle between the event axis and the x-y plane of the wireplane crack, the population of events is consistent with no CR-muon background. This is supported by the **MCNO\*** distribution of  $T_{\text{drift}}^{\text{Top}} - T_0$ , which exhibits a very strong peak at zero due to events erroneously pushed on the wireplane by the  $T_0$  algorithm. The obvious point to place the cut is at  $T_{\text{drift}}^{\text{Top}} - T_0 = 5 \text{ dtu}$ . However, in order to minimise the effect of the check-scan on real data, it was decided to exert a harsher cut: events with  $T_{\text{drift}}^{\text{Top}} - T_0 \leq 10 \text{ dtu}$  and  $\phi_x < 45^\circ$  are rejected. The acceptance is reduced by 33.9% for **BGD\*** and by 2.0% for **MCNO\*** when all other RINSE cuts have previously been applied.



• **Figure 5.7:** *CrZ*. View of a cosmic ray muon entering the main detector through the wireplane crack. The blob that pins the event on the wireplane is visible but has not been pulse-matched at this instance. The event is rejected.



• **Figure 5.8:** CrZ. Distribution of  $T_{\text{drift}}^{\text{Top}} - T_0$  (in dtu), where  $T_{\text{drift}}^{\text{Top}}$  is the time of the highest hit in the event box, for BGD\* (top); distribution of  $\phi_x$ , the angle between event axis and plane of the wireplane crack, versus  $T_{\text{drift}}^{\text{Top}} - T_0$  for BGD\* (middle); distribution of  $T_{\text{drift}}^{\text{Top}} - T_0$  for MCNO\* (bottom). All other RINSE cuts have already been applied in all three plots. The box shows where the cut is placed. The reader should note that the  $T_{\text{drift}}^{\text{Top}} - T_0$  distribution extends up to values of approximately 450 dtu.

- **CrY; Cathode Crack Cut**

A small fraction of cosmic ray muons are travelling close to the horizontal and may enter the detector through the cathode crack which lies in the x-z plane. The **BGD\*** distribution of  $C^{\text{Top}}$ , the cathode strip number of the highest hit in the event box, exhibits a small excess at the top of the bottom module which is correlated with  $A^{\text{Top}}$ , the anode channel of the same highest hit in the event box (fig 5.9).<sup>10</sup> Events with their highest hit on cathodes 235-239 and anodes 1-26 or 230-255, if the latter are external to the detector (as in the case of an L-shaped detector configuration), are rejected.

The acceptance is reduced by 2.5% for **BGD\*** and by 0.09% for **MCNO\*** when all other RINSE cuts have previously been applied.

### 5.3.4 The Data Quality Cuts

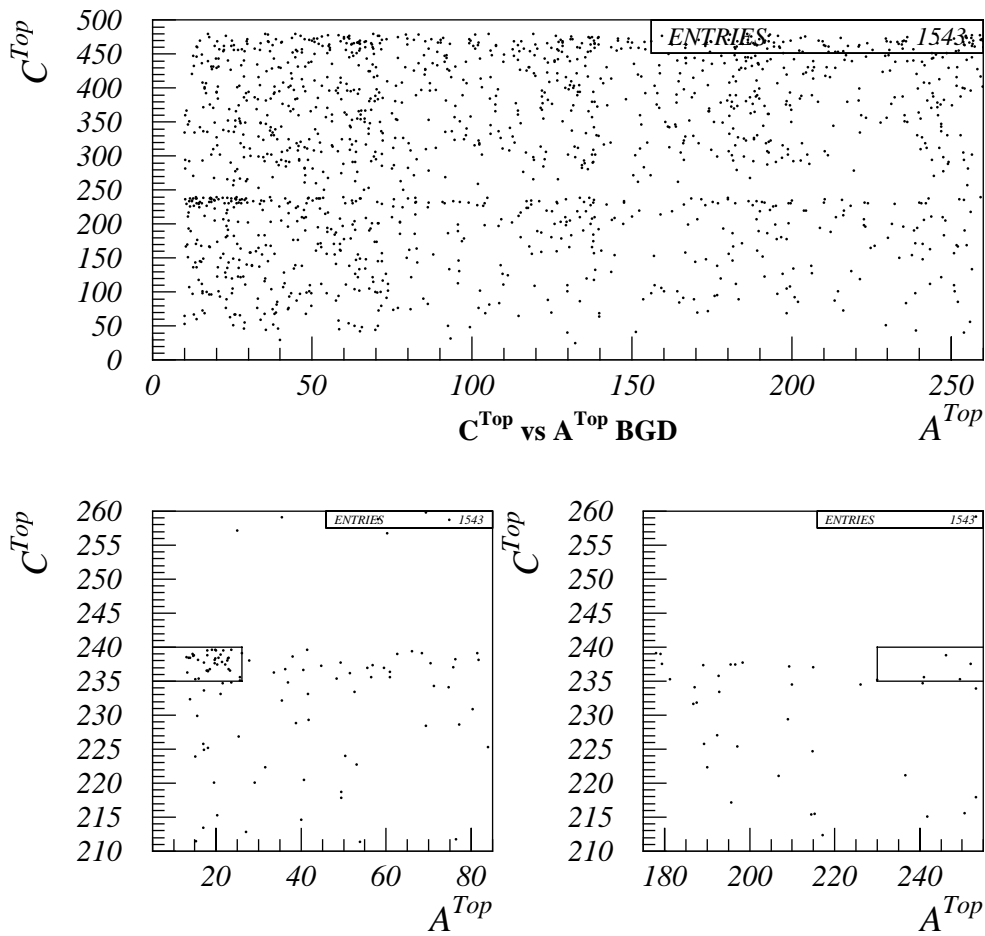
A variety of reasons may be responsible to reject an event by the quality criterion. These follow analytically.

- **CutQ4; Badly Reconstructed Events**

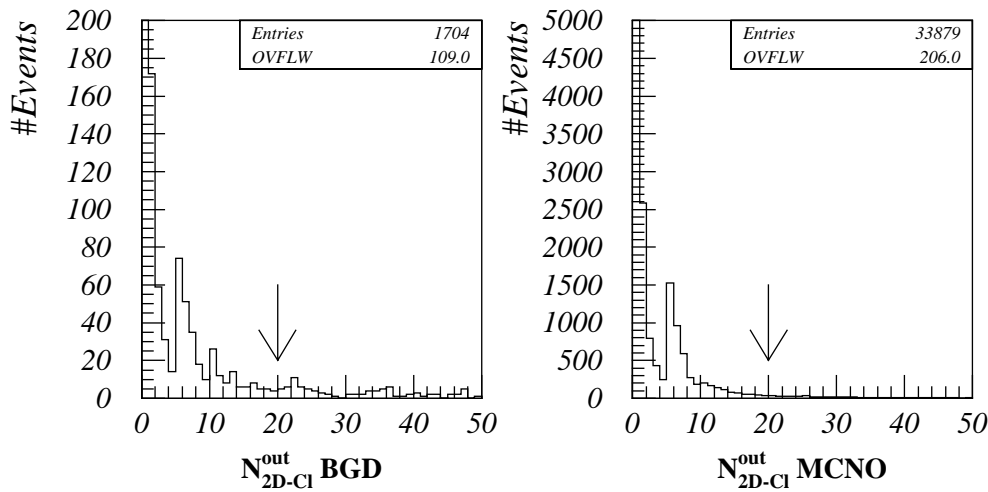
Cosmic-ray muons travelling in the x-y detector plane (which is normal to the drift direction) will produce *coincident* 2D pulses which are not efficiently matched by PMT. It is therefore possible that such events may have 2D pulses which cannot be projected within the boundaries of the event box. The **BGD\*** distribution of  $N_{2D-CI}^{\text{out}}$ , the sum of anode and cathode clustered 2D hits (see §3.3.2) which could not be mapped into the event box, exhibits a long tail relative to **MCNO\*** (fig 5.10). Events with  $N_{2D-CI}^{\text{out}}$  above 20 are rejected. The **BGD\*** and **MCNO\*** acceptances are reduced by 11.7% and 1.8% respectively when all other RINSE cuts have previously been applied.

---

<sup>10</sup> On the south and north faces the harsh fiducial volume cut has reduced **BGD** excess through the cathode crack.



• **Figure 5.9:** *CrY*. Scatter plot of  $C^{Top}$ , the cathode strip number of the highest hit in the event box, versus  $A^{Top}$ , the anode channel of the same hit, for **BGD\*** when all other RINSE cuts have already been applied (top). The concentration of events at the top of the lower modules and towards the outside of the detector is due to CR-muons entering the main detector via the Y-cracks on the east and west faces. The two lower plots are zoomed-in versions of the top plot and the boxes show where the cut is placed. Events on anodes 230-255 will only be rejected if these are external to the detector.



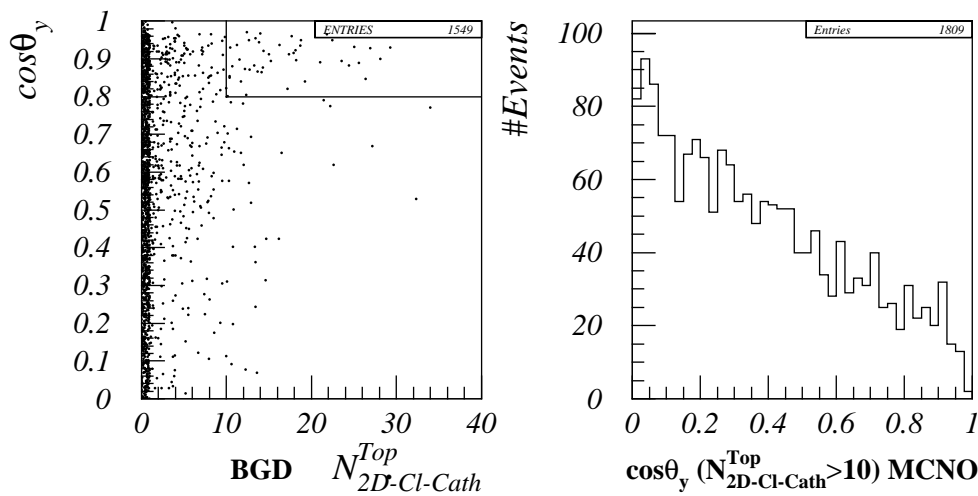
• **Figure 5.10: *CutQ4*.** Distribution of  $N_{2D-Cl}^{out}$ , the sum of anode and cathode clustered 2D hits which could not be mapped into the event box, for **BGD\*** (left) and **MCNO\*** (right) when all other RINSE cuts have previously been applied. Most events are at zero; the top of both plots has been clipped. Observe the very large overflows of the **BGD\*** distribution, due to badly matched events, primarily CR-muons travelling in the x-y plane. The arrows point to where the cut is placed.

#### • **CutQ5; Vertical Cosmic-Ray Muons**

A small fraction of cosmic-ray muons may enter the detector travelling in the z-y plane. This results in a string of cathode pulses matching to a single anode pulse at the top of the detector. PMT does not respond efficiently to this event topology and most of the cathode pulses at the top of the event, typically above cathode 400, remain unmatched. The muon eventually scatters in the detector and is better reconstructed. Chances are that it will be rejected by the fiducial volume cut as it leaves the detector from the bottom base. This cut is designed to reject such CR-muons that stop in the detector.

The **BGD\*** scatter plot of  $\cos \theta_y$ , where  $\theta_y$  is the angle between the event axis and the vertical, versus  $N_{2D-Cl\ Cath}^{Top}$ , the number of clustered unmatched cathode pulses above cathode 400, shows excess population for  $N_{2D-Cl\ Cath}^{Top} > 10$  and  $\cos \theta_y > 0.8$  (fig. 5.11). On the other hand, the **MCNO\*** acceptance decreases with increasing  $\cos \theta_y$  for  $N_{2D-Cl\ Cath}^{Top} > 10$

(fig. 5.11), which is the opposite from what has just been observed for **BGD\***. Hence, the **BGD\*** excess in that region is, indeed, attributed to CR-muons. Events with  $N_{2D-Cl\ Cath}^{Top} > 10$  and  $\cos\theta_y > 0.8$  are rejected. The **BGD\*** and **MCNO\*** acceptances are reduced by 2.8% and 0.5% respectively when all other RINSE cuts have previously been applied.



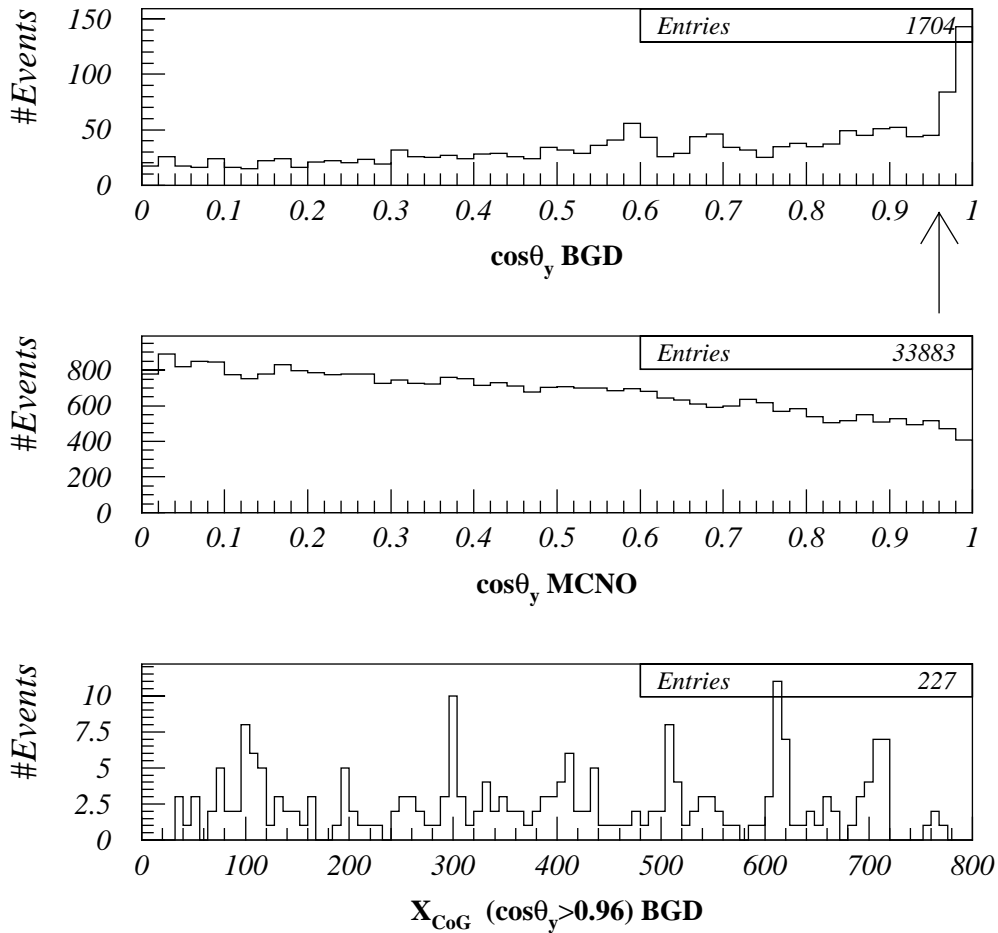
• **Figure 5.11: CutQ5.** Left: scatter plot of  $\cos\theta_y$ , where  $\theta_y$  is the angle between the event axis and the vertical, versus  $N_{2D-Cl\ Cath}^{Top}$ , the number of clustered unmatched cathode pulses above cathode 400, for **BGD\*** – the box encloses the rejected region. Right: **MCNO\***  $\cos\theta_y$  distribution with a cut of  $N_{2D-Cl\ Cath}^{Top} > 10$ . The **MCNO\*** expectation cannot predict the **BGD\*** excess at high  $\cos\theta_y$  and high  $N_{2D-Cl\ Cath}^{Top}$ . All other RINSE cuts have already been applied in both plots.

### • CutQ6; Crack Splats

A cosmic ray muon can travel straight down inter-modular cracks, sometimes producing bremsstrahlung radiation, which is seen as clusters of hits randomly distributed along the crack. This is a very characteristic pattern and is given the name of *crack splat*. The **BGD\*** distribution of  $\cos\theta_y$ , the angle between the event axis and the vertical, exhibits a very sharp peak for vertical events, not described by **MCNO\*** (fig 5.12). Interestingly, these events are found to cluster around the anode cracks (fig 5.12 bottom), which is very strong evidence for their crack-splat nature. We would also expect the same to happen for the wireplane cracks but this is harder to demonstrate because such small events are allowed to shift away from

the crack due to  $T_0$  failure – the  $T_0$  algorithm is optimised for neutrino interactions rather than background events. Since the anode and wireplane detector cracks are in the z-y and x-y planes respectively, events constrained in these planes by  $|\cos \theta_x| < 0.1$  or  $|\cos \theta_z| < 0.1$  and which have  $\cos \theta_y > 0.96$  will be rejected.

The **BGD\*** and **MCNO\*** acceptances are reduced by 11.7% and 2.8% respectively when all other RINSE cuts have previously been applied.



• **Figure 5.12: CutQ6.** Distributions of  $\cos \theta_y$ , the angle between the event axis and the vertical, for **BGD\*** (top) and **MCNO\*** (middle). The **BGD\*** distribution of  $X_{CoG}$ , the x-coordinate of the centre of gravity of the event, with  $\cos \theta_y > 0.96$  points to clustering around the anode cracks, every 100 cm, which corresponds to a module's width. All other RINSE cuts have already been applied.

- **CutTopA; CR-muons Coming Down Parallel to Anode Wires**

One of the hardest cases of non-contained events to reject is that of CR-muons entering the main detector in a vertical trajectory, parallel to and between anode wires, without leaving a trace in the drift tubes until they eventually scatter in the detector medium. The signature of these events is *their top pulses being at the same anode cable*. In the early stages of RINSE, such events were rejected at the check-scan level but it was soon realised that their characteristic topology is not uncommon to neutrino interactions and that the effect of the check-scan on neutrino data was not negligible. This was particularly worrying because the MC samples are not check-scanned and this introduced a systematic bias between real data and MC data. It was decided to apply an automated cut.

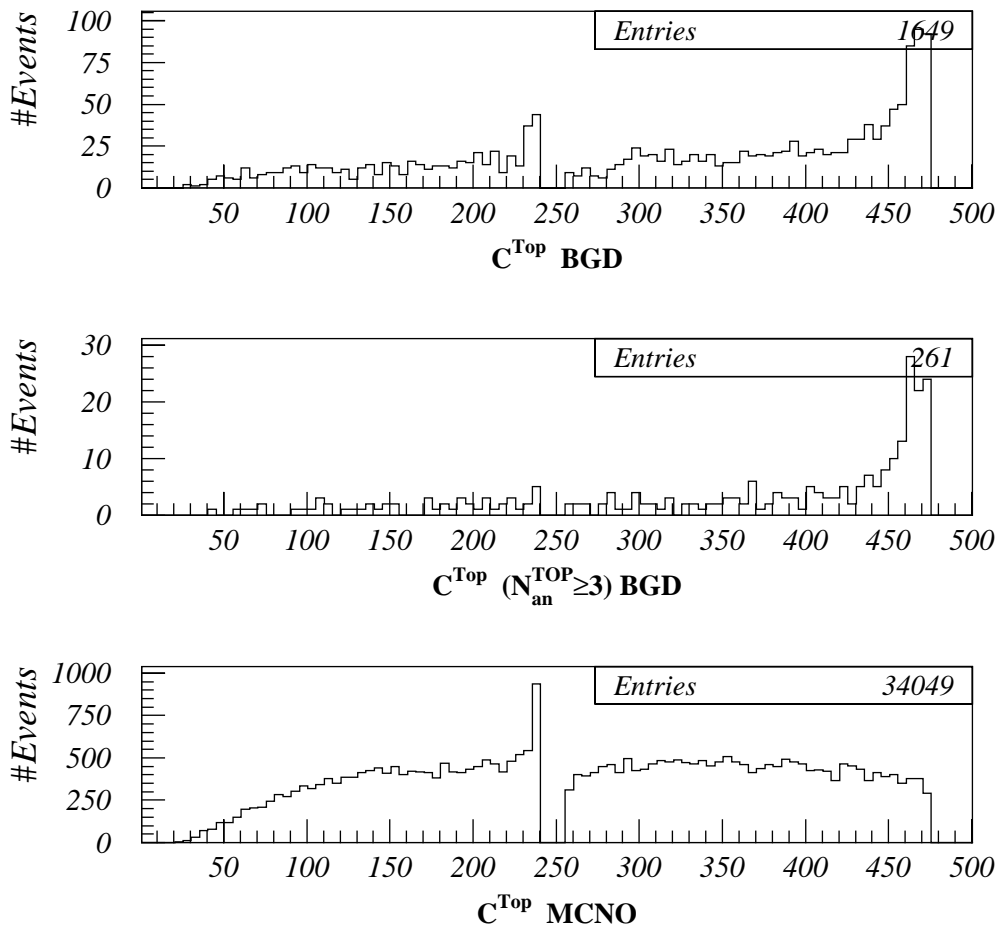
In order to address the issue,  $N_{\text{an}}^{\text{TOP}}$ , the number of the highest 5 hits in the event box lying on a single anode wire,<sup>11</sup> is introduced. It is observed that of the **BGD\*** events passing all other RINSE cuts, 15.8% have  $N_{\text{an}}^{\text{TOP}} \geq 3$ . The equivalent number for **MCNO\*** is 12.8%, pointing out the similarity of **BGD\*** and **MCNO\*** in this respect.

The cut concentrates on events which have  $N_{\text{an}}^{\text{TOP}} \geq 3$  because this is where the candidate CR-muon events travelling down between anode wires are found. It is observed that such **BGD\*** events cluster near the top of the detector (fig. 5.13). Indeed, this is a feature of the whole **BGD\*** sample that passes all other RINSE cuts, but is more pronounced for  $N_{\text{an}}^{\text{TOP}} \geq 3$ . The corresponding **MCNO\*** distribution does not exhibit this feature.

Of the **BGD\*** events with  $N_{\text{an}}^{\text{TOP}} \geq 3$  that pass all other rinse cuts, 55% have their highest hit above cathode 400. The corresponding number for **MCNO\*** is 18% (which is independent of  $N_{\text{an}}^{\text{TOP}}$ , of course).

---

<sup>11</sup> If two anode wires have the same population (such as two hits on one channel and two hits on another channel) the wire which is closest to the module's edge is chosen. Note that this is not necessary because this cut does not deal with cracks. However, it was thought best to be consistent for future reference and possible alterations to the algorithm.



• **Figure 5.13: *CutTopA*.** Distribution of the Cathode number of the highest hit in the event box for **BGD\*** (top), **BGD\*** with  $N_{an}^{TOP} \geq 3$  (middle) and **MCNO\*** (bottom). All other RINSE cuts have already been applied. The **BGD\*** excess near the detector top is obvious and becomes more pronounced with the cut on  $N_{an}^{TOP}$ .

Events which have  $N_{an}^{TOP} \geq 3$  and are high in the detector will be rejected. The rejection of **BGD\*** relative to **MCNO\*** is most efficient when the highest hit lies above cathode 450: 5.9% for **BGD\*** and 0.6% for **MCNO\*** (Table 5.2). Nevertheless, it was observed during check-scanning that vertical muons entering the main detector between anode wires appeared below cathode 450. In order to minimise bias between real data and MC it was decided to reject events if their highest hit is above cathode 400 and  $N_{an}^{TOP} \geq 3$ ; this corresponds to extending the fiducial volume cut to 95 cm from the top of the detector.

Highest hit Cathode range	$N_{\text{an}}^{\text{TOP}}$ range				
	1-5 (all events)	2-5	3-5	4-5	5
1-475	<i>1649 (100%)</i>	<i>883 (53.5%)</i>	<i>261 (15.8%)</i>	<i>91 (5.5%)</i>	<i>37 (2.2%)</i>
(all events)	<b>34049 (100%)</b>	<b>16652 (48.9%)</b>	<b>4345 (12.8%)</b>	<b>1312 (3.9%)</b>	<b>506 (1.5%)</b>
>300	<i>1014 (61.5%)</i>	<i>582 (35.3%)</i>	<i>189 (11.5%)</i>	<i>78 (4.7%)</i>	<i>34 (2.1%)</i>
	<b>15294 (44.9%)</b>	<b>7575 (22.2%)</b>	<b>2026 (6.0%)</b>	<b>633 (1.9%)</b>	<b>242 (0.7%)</b>
>350	<i>837 (50.8%)</i>	<i>498 (30.2%)</i>	<i>172 (10.4%)</i>	<i>70 (4.2%)</i>	<i>30 (1.8%)</i>
	<b>10597 (31.1%)</b>	<b>5218 (15.3%)</b>	<b>1394 (4.1%)</b>	<b>429 (1.3%)</b>	<b>163 (0.5%)</b>
>400	<i>637 (38.6%)</i>	<i>383 (23.2%)</i>	<i>144 (8.7%)</i>	<i>63 (3.8%)</i>	<i>27 (1.6%)</i>
	<b>5964 (17.5%)</b>	<b>2884 (8.5%)</b>	<b>781 (2.3%)</b>	<b>225 (0.7%)</b>	<b>90 (0.3%)</b>
>425	<i>531 (32.2%)</i>	<i>323 (19.6%)</i>	<i>124 (7.5%)</i>	<i>53 (3.2%)</i>	<i>26 (1.6%)</i>
	<b>3855 (11.3%)</b>	<b>1839 (5.4%)</b>	<b>478 (1.4%)</b>	<b>140 (0.4%)</b>	<b>55 (0.2%)</b>
>450	<i>369 (22.4%)</i>	<i>228 (13.8%)</i>	<i>97 (5.9%)</i>	<i>45 (2.7%)</i>	<i>24 (1.5%)</i>
	<b>1800 (5.3%)</b>	<b>842 (2.5%)</b>	<b>217 (0.6%)</b>	<b>63 (0.2%)</b>	<b>22 (&lt;0.1%)</b>

• **Table 5.2:** *CutTopA*. Number and fraction (in brackets) of events of the BGD\* (italics) and the MCNO\* (bold) event samples which fall within a range of  $N_{\text{an}}^{\text{TOP}}$  for a given range of the Cathode of their highest hit in the event box. All other RINSE cuts have already been applied. The shaded column is for  $N_{\text{an}}^{\text{TOP}} \geq 3$ , where most of the vertical muons that enter the main detector by travelling between anode wires are expected to lie.

With this cut the BGD\* acceptance is reduced by 8.7% while the MCNO\* acceptance is reduced by 2.3% when all other RINSE cuts have previously been applied.

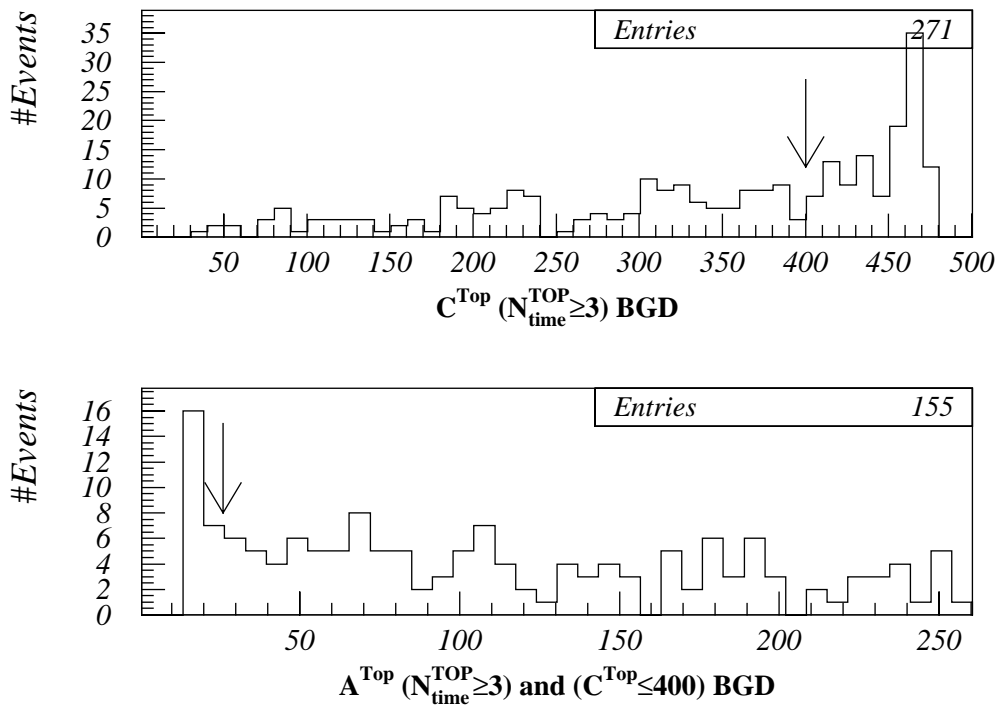
Finally, note that for this cut one is not concerned with the north/south faces of the detector because of the harsher fiducial volume cut applied at the end-looms.

• **CutTopT; Events with Blob not Identified by BLOBER**

It is observed that, despite the existence of a blob, single-loom events may be sometimes misplaced at the module centre, because of a failure of the  $T_0$  algorithm, which is usually due to random noise hits. A pulse-matched blob at the top of the event will indicate a charged particle which probably came down through a wireplane crack. Such events were

originally rejected at the check-scan level but, similarly to the previous cut, a software algorithm was devised.

We examine  $N_{\text{time}}^{\text{TOP}}$ , the number from the highest 5 hits in the event box that are coincident, where coincidence is defined empirically within a time window of 2 dtu. Remarkably, the distributions of  $N_{\text{time}}^{\text{TOP}}$  differ little between BGD\* and MCNO\*; 17% of BGD\* and 12% of MCNO\* events have  $N_{\text{time}}^{\text{TOP}} \geq 3$ . We concentrate on these events because they are candidates with blob structure at their top. In the BGD\* sample they show an excess at the top (high cathode number) and east/west sides (low anode number) of the detector (fig. 5.14). An event is rejected if  $N_{\text{time}}^{\text{TOP}} \geq 3$  and its highest hit is above cathode 400 or on anode



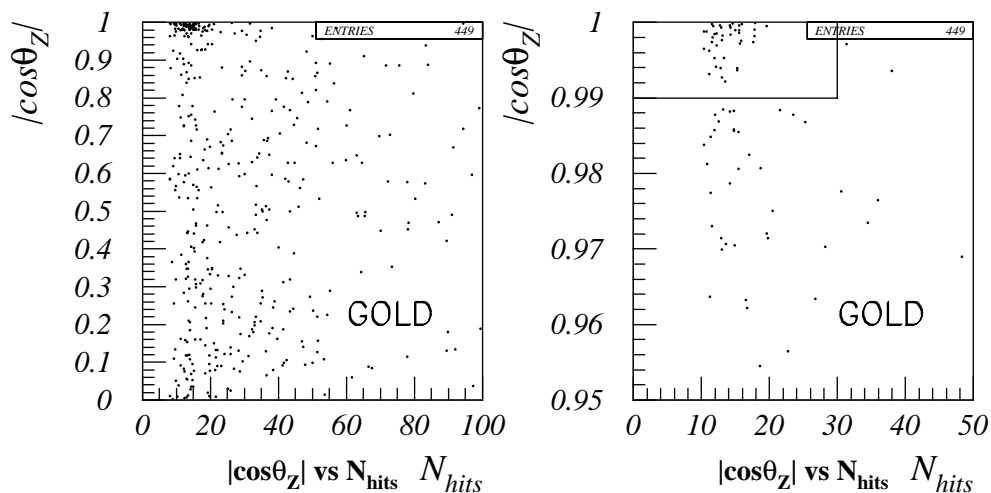
• **Figure 5.14: *CutTopT*.** Distribution of the Cathode channel (top) and the Anode channel (bottom) for BGD\* events with  $N_{\text{time}}^{\text{TOP}} \geq 3$  and all other RINSE cuts applied. For the bottom plot, events with the Cathode channel of their highest hit above 400 have also been rejected in order to enhance the effect of the cut. The arrows show where the cuts on these two quantities are set. The corresponding distributions for MCNO\* (not shown) are flat, when allowing for phase-space effects.

channels 14-26 or 229-241, if the latter are external to the detector. In other words, the fiducial volume cut is extended to 95 cm from the top and to 40 cm from the east/west faces of the detector when  $N_{\text{time}}^{\text{TOP}} \geq 3$ . The above cut rejects 5.7% of the BGD\* sample and 1.5% of the MCNO\* sample when all other RINSE cuts have previously been applied.

Note that *CutTopT* is also a harsh cut in order to minimise systematic biases that may occur between real data and MC data because of the check-scan, not unlike the previous cut, *CutTopA*.

- **CutBreak; Class of Breakdown Events**

The GOLD\* data exhibits high concentration of small events whose event axis is very well aligned with the drift direction (fig. 5.15). This excess is unphysical and not described by MCNO\* and is attributed to a class of breakdown events whose most characteristic pattern is a series of hits in the same drift tube. These events are due to module malfunction and are not correlated with the shield activity, which is why they are seldom found in the BGD\*



- **Figure 5.15: CutBreak.** Scatter plot of the absolute value of cosine of  $\theta_z$ , the angle between the event axis and the drift ( $z$ ) axis, and  $N_{\text{Hits}}$ , the number of 3D hits in the box, for GOLD\* when all other RINSE cuts have previously been applied (left). A concentration is observed for small events whose axis is parallel to the drift direction. The zoomed-in plot (right) illustrates where the cut is placed.

sample. Events with  $|\cos \theta_z| > 0.99$ , where  $\theta_z$  is the angle between the event axis and the  $z$  (drift) axis, and  $N_{\text{Hits}} < 30$ , where  $N_{\text{Hits}}$  is the number of 3D hits in the event box, are rejected. The **GOLD\*** and **MCNO\*** acceptances are reduced by 8.9% and 0.5% respectively when all other RINSE cuts have previously been applied.

- **CutSnake; Snake Cut**

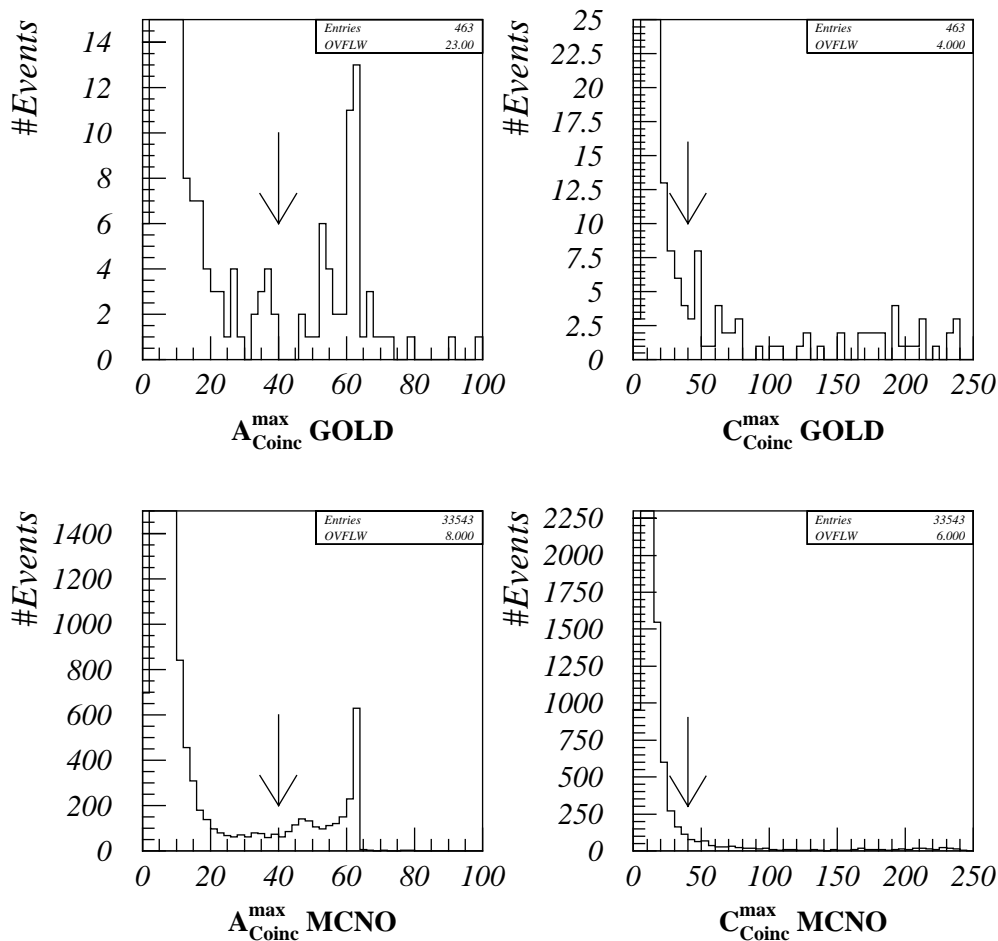
Snakes are very large breakdown events, which are due to a high voltage discharge in the detector. Their layout is very characteristic in that they consist of a group of coincident pulses in all the anode or cathode channels in a module or even in a whole loom. All the coincident pulses count as a single pulse “edge” and do not trigger the detector. Snakes may appear superimposed in the time frame of contained events. Only a very small fraction of snakes, to be referred to as *supersnakes*, can trigger the detector on their own. Their very large breakdown pulses have oscillating amplitude and, as they die out, form tail pulses by going below detection threshold and back up again, thus creating multiple edges to which the trigger is sensitive.

Supersnakes are not correlated with shield activity and are mostly found in the **GOLD\*** sample. The **GOLD\*** distributions of  $A_{\text{Coinc}}^{\text{max}}$  and  $C_{\text{Coinc}}^{\text{max}}$ , the largest populations of coincident 2D pulses on a single anode and cathode channel respectively, have long tails which are not reproduced by **MCNO\*** (fig. 5.16). These are attributed to snakes and an event with  $A_{\text{Coinc}}^{\text{max}} > 40$  or  $C_{\text{Coinc}}^{\text{max}} > 40$  is an anode or cathode supersnake candidate. Note that  $A_{\text{Coinc}}^{\text{max}}$  and  $C_{\text{Coinc}}^{\text{max}}$  are measured in loom space and range within 1-252 and 1-478 respectively. The small peak at  $A_{\text{Coinc}}^{\text{max}} = 63$  for both **GOLD\*** and **MCNO\*** samples is due to snakes which are contained within a module. The snakes in **MC** event samples come from the **PULSER** events on which the **MC** neutrino events are superposed.

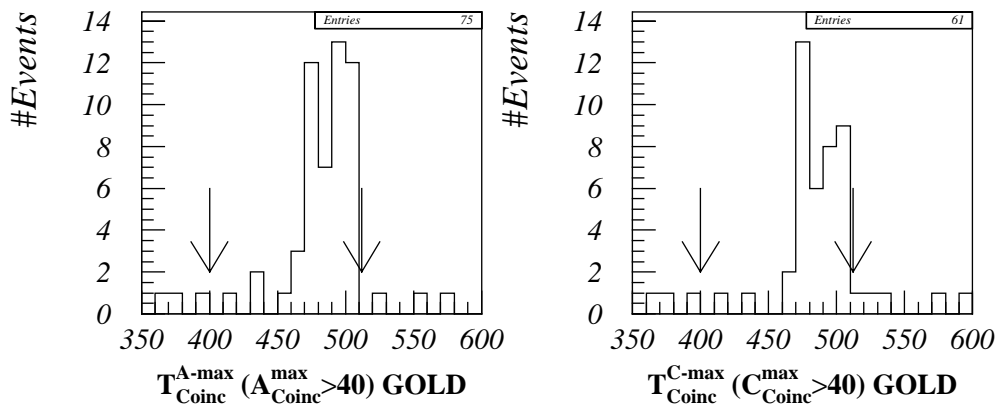
In order to trigger the detector, supersnakes must occur close to (and before) the trigger time. The distributions of  $T_{\text{Coinc}}^{\text{A-max}}$  and  $T_{\text{Coinc}}^{\text{C-max}}$ , the times at which the populations  $A_{\text{Coinc}}^{\text{max}}$  and  $C_{\text{Coinc}}^{\text{max}}$  respectively occurred, indicate that the **GOLD\*** supersnake candidates occur in a time-window of 450 to 511 dtu, the latter being the trigger time, for both the anodes and

the cathodes (fig. 5.17). However, it was observed in the check-scan that some supersnakes occurred just below 450 dtu and it was decided to enlarge the supersnake time-window from 400 to 511 dtu.

Events with  $A_{\text{Coinc}}^{\text{max}} > 40$  and  $400 < T_{\text{Coinc}}^{\text{A-max}} < 512$  or events with  $C_{\text{Coinc}}^{\text{max}} > 40$  and  $400 < T_{\text{Coinc}}^{\text{C-max}} < 512$  are rejected. The GOLD\* and MCNO\* acceptances are reduced by 11.7% and 0.8% respectively when all other RINSE cuts have previously been applied.



• **Figure 5.16: CutSnake.** Distributions of  $A_{\text{Coinc}}^{\text{max}}$  and  $C_{\text{Coinc}}^{\text{max}}$ , the largest populations of coincident 2D pulses on a single anode and cathode channel respectively, for GOLD\* (top) and MCNO\* (bottom). All other RINSE cuts have already been applied. The arrows point to the supersnake cut in these variables.

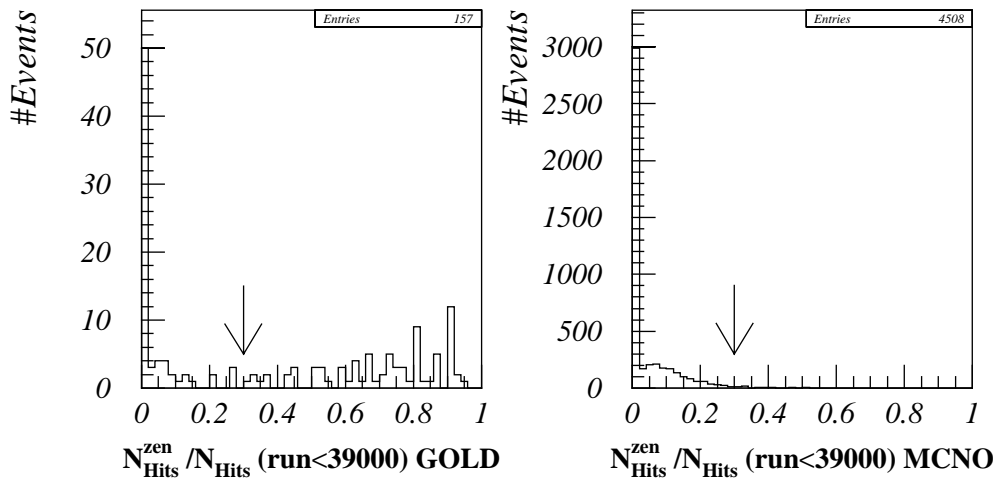


• **Figure 5.17: CutSnake.** Distributions of  $T_{\text{Coinc}}^{\text{A-max}}$  (left) and  $T_{\text{Coinc}}^{\text{C-max}}$  (right), the times at which the populations  $A_{\text{Coinc}}^{\text{max}}$  and  $C_{\text{Coinc}}^{\text{max}}$  respectively occurred, measured in dtu, for **GOLD\*** supersnake candidates. All other RINSE cuts have previously been applied. The arrows point to the limits of the supersnake time-window.

#### • CutZen; Zen Cut

Zens preoccupied the Soudan 2 Collaboration in the early days of the experiment. They are small events that occur on particular cathode channels and the whole range of anode channels. It was soon realised that the existence of zens was due to a design feature of the modules constructed at Argonne laboratory: every 32 cathode strips are fixed on 35 cm high boards, which, when mounted on the module, are separated by a 2-3 mm gap. Ionisation deposited on the back face of the cathode boards can drift through this gap and be recorded because of the weak fringe fields from the anode cables that extend into this region. Because of their extended time structure, zens can trigger the detector. Zens indeed occur on the two cathode channels on either side of the gap between cathode boards in Argonne modules. Over the frequent refurbishment operations on the detector, these gaps were covered with a strip of Mylar. The cathode strips in the UK-constructed modules are fixed on a large, single board and, as expected, are found to be zen-free.

Zens are not correlated with shield activity: most of them appear in the **GOLD\*** sample. The earliest **GOLD\*** data analysed in this thesis, before run 39000, has many events



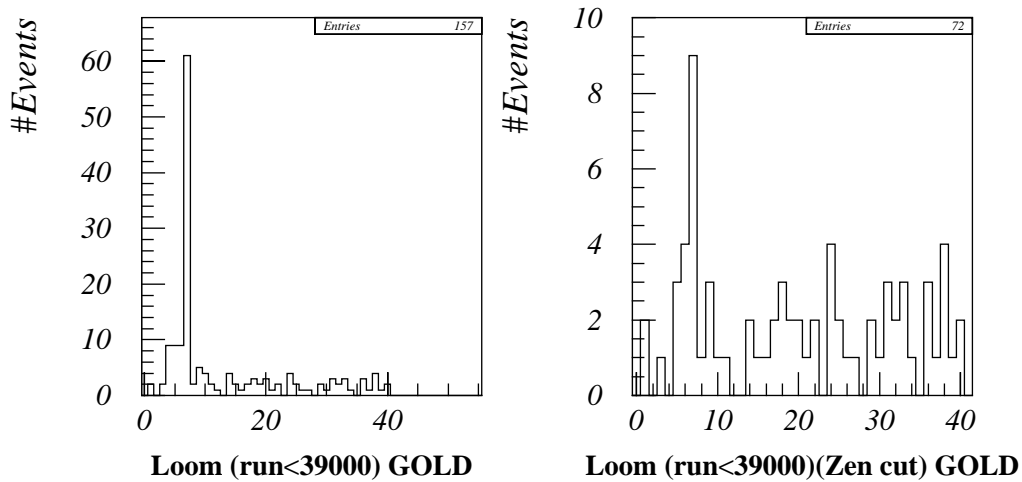
• **Figure 5.18:** *CutZen*. Distribution of the ratio of  $N_{\text{Hits}}^{\text{zen}}$ , the number of 3D hits in the box on zen channels, to  $N_{\text{Hits}}$ , the total number of 3D hits in the box, for **GOLD\*** (left) and **MCNO\*** (right). All other RINSE cuts have previously been applied. The arrows point to the value of the cut.

with a high fraction of their 3D hits on zen channels, which is incompatible with **MCNO\*** (fig. 5.18). Events before run 39000 with 30% or more of their 3D hits on zen channels are rejected. The **GOLD\*** and **MCNO\*** acceptances are reduced by 17.2% and 0.2% respectively when all other RINSE cuts have previously been applied.

It is worth pointing out that before run 39000 certain detector regions, such as loom 8, were particularly active; their population has been dramatically reduced after applying the zen cut (fig. 5.19).

#### • **CutHit; Number of Hits (Energy) Cut**

The comparison of the hit distributions for **GOLD\*** and **MCNO\*** clearly points to a very large excess in the data for small events (fig 5.20). This is attributed to detector noise and breakdowns. Events having 10 or less 3D hits are rejected. Ten hits correspond to  $\approx 300$  MeV (see §6.3). Excess in the data is still noticeable for events of up to 25 hits and is also attributed to detector breakdowns. Because they have a very characteristic pattern that

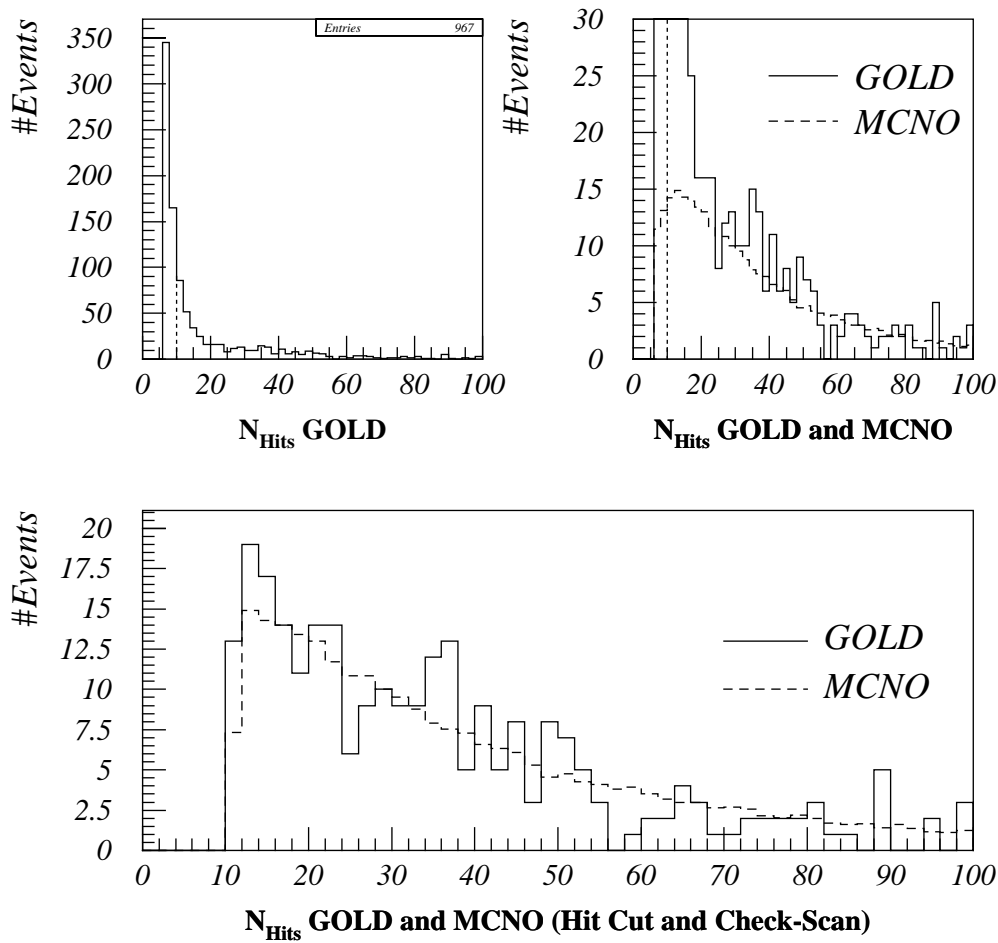


• **Figure 5.19:** *CutZen*. Population of detector looms for **GOLD\*** data before run 39000 (left) when all other RINSE cuts have previously been applied. For the plot on the right the zen cut has also been applied: the population of the previously “hot” looms has been suppressed.

is quite unlike a neutrino induced event, it was decided to have them removed at the check-scan stage, after which the final **GOLD** and **MCNO** hit distributions agree well (fig 5.20).

After the 10-hit cut, the **GOLD\*** and **MCNO\*** acceptances are reduced by 57.7% and 10.2% respectively when all other RINSE cuts have previously been applied.

The rejection of low energy events contradicts one of the strengths of the Soudan 2 detector against the water Čerenkov detectors: its lower energy threshold for heavy charged particles. On the other hand, very low energy (below 300 MeV) neutrino interactions carry very little flavour information and no direction information; the latter is washed out by nuclear Fermi momentum, typically of the order of 250 MeV/c [47]. It is therefore believed that the Hit cut will have a minimal effect on the investigation of the atmospheric neutrino problem, where both the neutrino flavour and direction are quantities of interest.



• **Figure 5.20: CutHit.** Distributions of the number of 3D hits in the event box: **GOLD\*** with all other RINSE cuts already applied (top left); the same is repeated with **GOLD\*** (top clipped off) and **MCNO\*** (normalised to the data exposure by 1/116) superposed. The bottom plot presents the final **GOLD** and **MCNO** (normalised by 1/116) hit distributions when all RINSE cuts, including the hit cut and the check-scan, have been applied.

- **CutRun; Faulty Runs Cut**

The sets of runs where the detector malfunctioned was inferred by the very large numbers of CEVs that passed the RINSE containment cuts. The faulty run ranges are (inclusive):

- 31011-31105; gas rack 3 was leaking.
- 31670; half-walls 1 to 15 and 18 had a high voltage trip.
- 49975-50013; high voltage sweep at  $-150$  V off the nominal value of 9 KV. In order to optimise each module for minimum noise and maximum drifting efficiency, the detector operation was monitored under different values of drift voltage during December 1993. It turned out that, from the drifting point of view,  $-150$  V off the nominal value was too low for most of the detector modules.
- 50419-50533; gas rack 4 malfunction and severe leakage.

These runs are rejected from both data and MC event samples. The **BGD\***, **GOLD\*** and **MCNO\*** acceptances are reduced by 20.3%, 2.4% and 0.5% respectively when all other RINSE cuts have previously been applied. It is worth pointing out that there were no such major faults since December 1993, which is to the credit of the mine-crew who take care of the detector.

### **5.3.5 Summary of Automated RINSE Containment Cuts**

The presentation of the automated RINSE containment cuts has been completed. A summary of their performance is given in Table 5.3, where the number of events rejected by each cut alone is listed for **GOLD**, **BGD** and **MCNO**. The fiducial volume, crack (anode and wireplane) and hit cuts are the most powerful here.

CUT	MCNO	GOLD	BGD
	<b>Number of events passing all RINSE cuts (excl. Check-Scan)</b>		
<b>All RINSE (excl. Check-Scan)</b>	33268	409	1505
	<b>Number of events failing only this RINSE cut</b>		
<b>CutE1</b>	26 (<0.1%)	6 (1.4%)	6 (0.4%)
<b>CutE2</b>	354 (1.1%)	47 (10.3%)	43 (2.8%)
<b>CutFV</b>	3886 (10.5%)	96 (19.0%)	1903 (55.8%)
<b>CrX</b>	1273 (3.7%)	84 (17.0%)	1861 (55.3%)
<b>CrZ</b>	685 (2.0%)	54 (11.7%)	773 (33.9%)
<b>CrY</b>	31 (<0.1%)	5 (1.2%)	38 (2.5%)
<b>CutQ4</b>	611 (1.8%)	29 (6.6%)	199 (11.7%)
<b>CutQ5</b>	177 (0.5%)	1 (0.2%)	44 (2.8%)
<b>CutQ6</b>	615 (1.8%)	16 (3.8%)	199 (11.7%)
<b>CutTopA</b>	781 (2.3%)	22 (5.1%)	144 (8.7%)
<b>CutTopT</b>	514 (1.5%)	23 (5.3%)	91 (5.7%)
<b>CutBreak</b>	171 (0.5%)	40 (8.9%)	12 (0.8%)
<b>CutSnake</b>	275 (0.8%)	54 (11.7%)	54 (3.5%)
<b>CutZen</b>	67 (0.2%)	85 (17.2%)	30 (2.0%)
<b>CutHit</b>	3795 (10.2%)	558 (57.7%)	606 (28.7%)
<b>CutRun</b>	167 (0.5%)	10 (2.4%)	384 (20.3%)

• **Table 5.3:** Number of events passing all RINSE containment cuts, excluding the Check-Scan, (top) and failing only one of the RINSE cuts (below) for **MCNO**, **GOLD** and **BGD**. The number in brackets is the loss of acceptance for each cut when all other cuts in the table have already been applied.

### 5.3.6 The Check-Scan

The very last stage in the RINSE chain of containment cuts is the check-scan. It is important to point out that this is a process unique to the real data (both **GOLD** and **BGD**) and is not applied to the very large **MC** sample. For this reason, the effect of the check-scan on the real neutrino sample *must* be minimal: the scanner only rejects events which are certainly not due to a neutrino interaction in the main detector. In this category lie the cosmic ray muons, which have passed the RINSE containment cuts because of small detector malfunctions or because of the presence of noise hits (natural radioactivity etc.), as well as detector breakdown events. All the contained events are classified as such and a “dubious” category, when the scanner cannot decide with certainty upon the nature of the event, is optional. In order to minimise any systematic effects due to human bias, the **GOLD** and **BGD** samples are mixed together and are scanned shield-blind, without the scanner knowing their identity.

The check-scan is carried out independently by two experienced physicists. Their scan matrix determines which events pass to the final **GOLD** and **BGD** samples, to be used in the flavour analysis along with the **MCNO** and **MCAF** samples. In this exercise Hugh Gallagher and myself scanned the whole data-set, but for runs 30000-38999 where I was replaced by Wade Allison.

In order to substantiate the check-scanning procedure, it was deemed necessary to perform this task on a small **MC** sample. This was done while check-scanning the data for runs 70000-74999. A small sample of **MCNO** events was randomly picked from the corresponding **MC** data-set for this period and was mixed with the real data. The resultant event sample was check-scanned **MC**-blind and shield-blind. Tables **5.4** to **5.6** contain the scan matrices comparing the decisions of the two scanners for the RINSEd **GOLD**, **BGD** and **MCNO** samples respectively.

It is apparent from the **MCNO** scan matrix that only a small fraction of the neutrino sample is rejected by the check-scan procedure (Table **5.6**). Statistics are low, but approximately 6% of the events are rejected when events scanned as CEV by *both* scanners

are passed to the final MCNO sample. The rejected fraction is reduced to 2% when events scanned as CEV by *either* scanner are accepted in the final MCNO sample.

The population of the final BGD sample will increase from 666 events, when both scanners have to agree on a CEV, to 865 events, when one scanner's nod of approval is enough for an event to be accepted (Table 5.5). Relative to the former case, the background contamination of the GOLD sample will increase by 28.5% when events chosen as CEV by either scanner are accepted.

In order to reduce the systematic uncertainty on the flavour analysis due to the fact that the MC sample is not check-scanned, it was decided to *accept events that were passed as CEV by either scanner*. Events flagged as breakdowns by at least one scanner are rejected. The background contamination of GOLD may increase but the data-MC systematic biases are reduced by a factor of 3.

The acceptance of the check-scan procedure is 68.6% for GOLD, 56.9% for BGD, and 97.9% for the small fraction of MCNO that was put through the test.

### 5.3.7 The Shield Cuts

The shield cuts – which had not been defined but were used in the definition of the containment cuts in the previous sections – will divide the contained event sample, which has been selected from the RINSE containment cuts (including the check-scan) into the final GOLD and BGD samples. A neutrino candidate in the GOLD event sample must not have any shield activity associated with it. The contained events vetoed by the shield will form the BGD sample which will be studied in order to estimate the contamination of GOLD from CR-muons and their interactions in the rock surrounding the main detector.

Only shield adjacencies and overlaps (see §3.1.3) will be considered in the following discussion on the shield cuts. No distinction will be made between the two. The random rate of single shield hits is too large to be useful (see §3.1.3). The variables that will be used in the definition of the shield cuts are:

GOLD		Scanner 1 – AS (WWMA)			
Scanner 2 - HRG		CEV	CR-muon	Dubious	Breakdown
	CEV	256	5	6	3
	CR-muon	6	26	1	1
	Dubious	7	5	4	5
	Breakdown	1	1	1	81

• **Table 5.4:** Check-scan matrix for **GOLD** sample, runs 30000-74999, 409 events, 280 pass.

BGD		Scanner 1 – AS (WWMA)			
Scanner 2 - HRG		CEV	CR-muon	Dubious	Breakdown
	CEV	666	65	40	3
	CR-muon	35	510	19	0
	Dubious	50	62	19	3
	Breakdown	2	4	1	26

• **Table 5.5:** Check-scan matrix for **BGD** sample, runs 30000-74999, 1505 events, 856 pass.

MCNO		Scanner 1 – AS (WWMA)			
Scanner 2 - HRG		CEV	CR-muon	Dubious	Breakdown
	CEV	177	1	1	0
	CR-muon	2	2	0	0
	Dubious	4	2	0	0
	Breakdown	0	0	0	0

• **Table 5.6:** Check-scan matrix for fraction of **MCNO** sample, runs 70000-74999, 189 events.

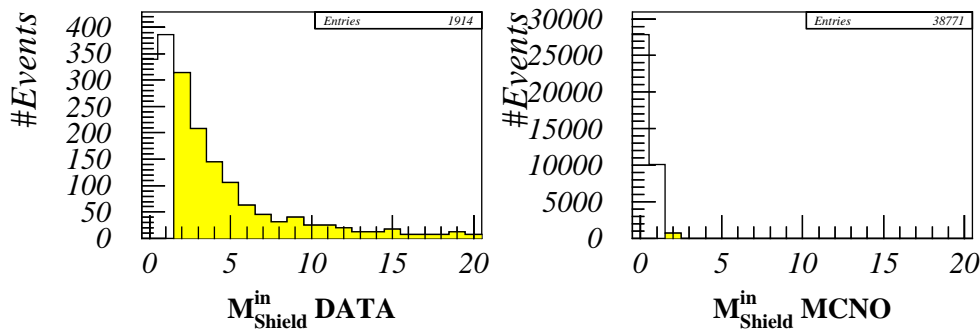
- $M_{\text{Shield}}^{\text{in}}$ , the *shield multiplicity inside the  $T_0$ -window*, defined as the largest number of coincident shield hits in the time range of the  $T_0$ -window.
- $M_{\text{Shield}}^{\text{out}}$ , the *shield multiplicity outside the  $T_0$ -window*, defined as the largest number of coincident shield hits outside the time range of the  $T_0$ -window.
- $D_{\text{Sh-Box}}^{\text{min}}$ , the *minimum distance in the detector volume* along a direction joining any one of the shield hits and any of the 8 corners of the event box. This is calculated for the group of shield hits with the greatest multiplicity inside the  $T_0$ -window. If there exist two groups of shield hits with the same value of  $M_{\text{Shield}}^{\text{in}}$  occurring at different times, then the group with the minimum  $D_{\text{Sh-Box}}^{\text{min}}$  is the one used in the following analysis.

- **CutSh2: Shield Multiplicity of 2 and Above**

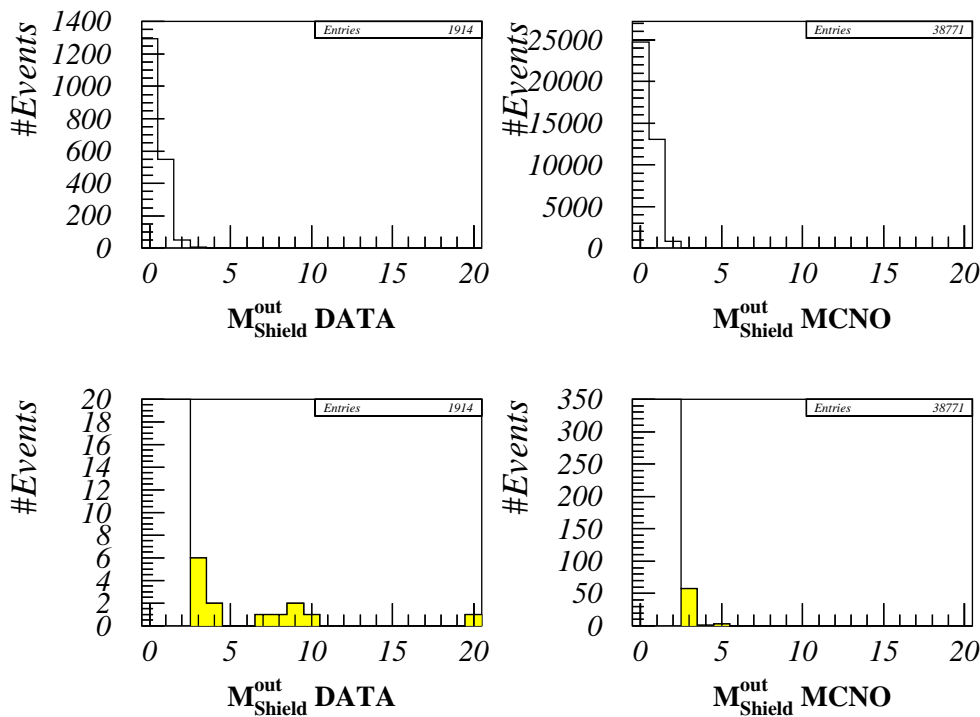
It is observed that 62.1% of the **DATA** events have  $M_{\text{Shield}}^{\text{in}}$  of 2 or above (fig. 5.21). On the other hand, only 2.0% of the **MCNO** sample falls in that region, because this requires a random coincidence in the shield activity (coming from **PULSER** data on which **MC** events are superimposed). For this reason, all events with  $M_{\text{Shield}}^{\text{in}} \geq 2$  are rejected from **GOLD** and are classified as **BGD** candidates.

The  $T_0$ -window defines the range of time within which the event may lie and shield hits occurring outside that range are thought to be irrelevant with the event. Hence, the distributions of  $M_{\text{Shield}}^{\text{out}}$  for the **DATA** and **MC** samples should be similar. However, the **DATA** shows small relative excess to **MCNO** for large values of  $M_{\text{Shield}}^{\text{out}}$ : 1% of the **DATA** and only 0.2% of **MCNO** have  $M_{\text{Shield}}^{\text{out}} \geq 3$  (fig. 5.22). This small difference is attributed to non-neutrino-like events where the  $T_0$ -window algorithm has failed. Events with  $M_{\text{Shield}}^{\text{out}} \geq 3$  are rejected from **GOLD** and classified as **BGD** candidates.

After *CutSh2*, the **GOLD** and **MCNO** acceptances are reduced by 74.6% and 2.4% respectively when all other **RINSE** cuts (including *CutSh1*) have previously been applied.



• **Figure 5.21:** *CutSh2*. Shield multiplicity in the  $T_0$ -window for **DATA** (left) and **MCNO** (right). All RINSE containment cuts have already been applied. The shaded areas are rejected.

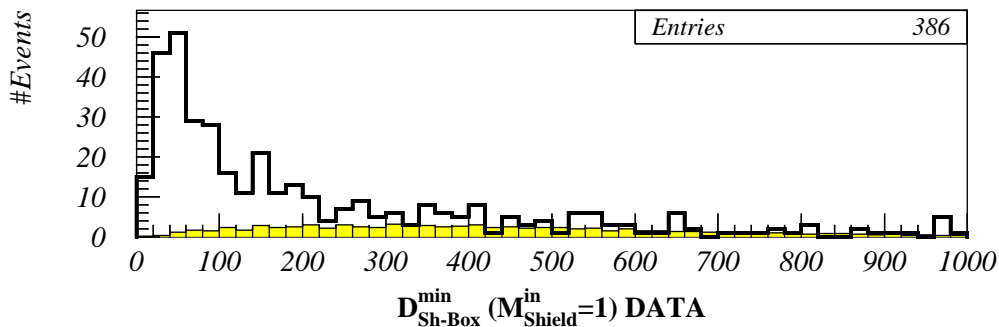


• **Figure 5.22:** *CutSh*. Shield multiplicity outside the  $T_0$ -window for **DATA** (top left) and **MCNO** (top right). The same is repeated with the histograms' top clipped to approx. 1.5% of their maximum value (bottom plots). All RINSE containment cuts have already been applied. The shaded areas are rejected.

- **CutSh1: Unit Shield Multiplicity**

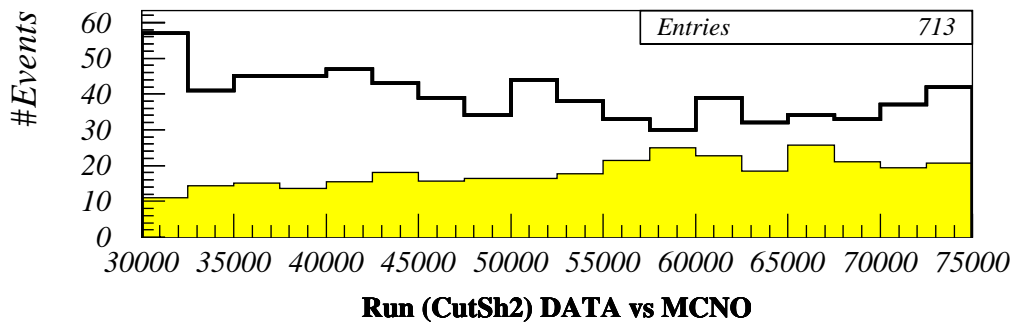
The case of unit shield multiplicity inside the  $T_0$ -window is less straightforward. As many as a *quarter* of the MC sample fall in this category (fig. 5.21) and their rejection would have a major effect on the acceptance. On the other hand the DATA clearly exhibits an excess, due to CR muons firing off just one shield hit.<sup>12</sup>

One expects spatial correlation between shield hit and associated event in the main detector. The distributions of  $D_{\text{Sh-Box}}^{\text{min}}$  for DATA against MCNO shows the clear DATA excess for values of  $D_{\text{Sh-Box}}^{\text{min}}$  up to 5 m (fig. 5.23), a figure that cannot be attributed to a physical process because it corresponds to many interaction lengths in the detector. Nevertheless, it can be understood by the fact that the shield was more inefficient in the early days of the experiment (see §3.1.3). The distribution of run numbers before applying the unit shield multiplicity cut shows excess in DATA relative to MCNO which is more pronounced in the early days of the experiment (fig. 5.24). The excess itself is due to the fact that CR-muon



• **Figure 5.23: CutSh1.** Distribution of  $D_{\text{Sh-Box}}^{\text{min}}$  for DATA (thick line) and MCNO normalised to the data exposure by 1/116 (shaded area) when  $M_{\text{Shield}}^{\text{in}} = 1$ . All RINSE containment cuts (excluding the check-scan) have been applied.

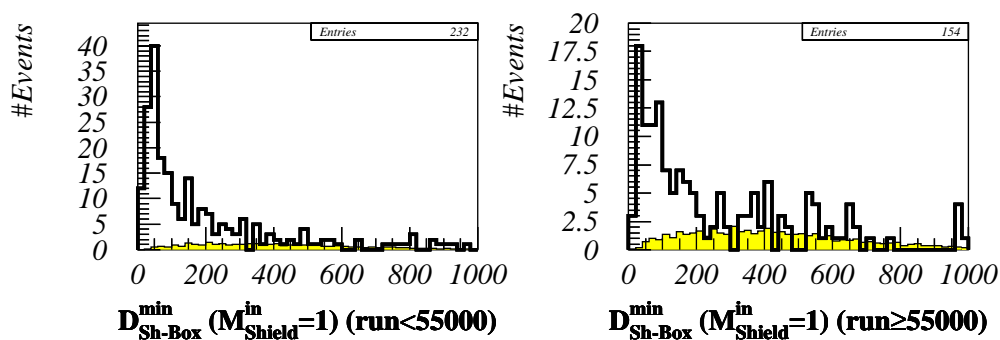
<sup>12</sup> The scanning team classifies the unit shield multiplicity events into their BGD sample. Their loss of acceptance is smaller because (i) they have a tighter  $T_0$  window set by hand and (ii) they only consider adjacencies (and not overlaps) as shield activity and their random rate is lower.



• **Figure 5.24:** *CutSh1*. Distribution of run number for **DATA** (thick line) and **MCNO** normalised to the data exposure by 1/116 (shaded area). All RINSE containment cuts (excluding the check-scan) and *CutSh2* have been applied.

events coming through the shield and leaving one hit or no hit at all have not yet been rejected. The fact that a greater surplus occurs in the early data is a statement of the poorer shield performance in these days. On the basis of this argument, the **DATA** is divided into two parts, before and after run 55000.

The **DATA** and **MC** distributions of  $D_{\text{Sh-Box}}^{\text{min}}$  with  $M_{\text{Shield}}^{\text{in}} = 1$  for these two periods support the above (fig. 5.25). In the early era, the **MCNO** population is scarce relative to the

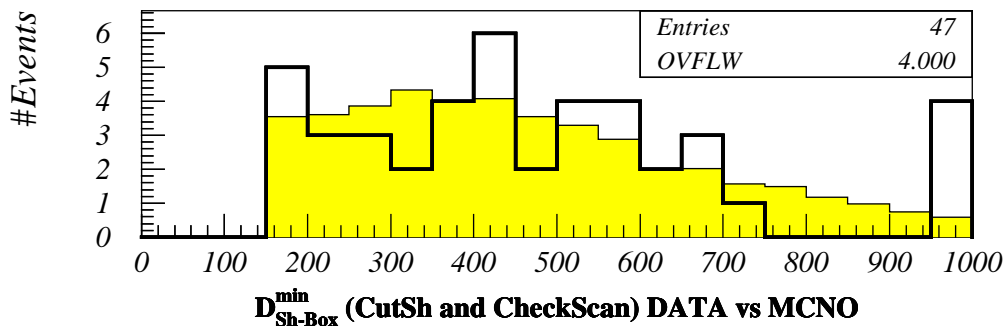


• **Figure 5.25:** *CutSh1*. Distributions of  $D_{\text{Sh-Box}}^{\text{min}}$  when  $M_{\text{Shield}}^{\text{in}} = 1$  for runs before and after 55000 (left and right respectively) for **GOLD** (thick line) and **MCNO** normalised to the data exposure by 1/116 (shaded area). All RINSE containment cuts (excluding the check-scan) have already been applied.

**DATA:** events with  $M_{\text{Shield}}^{\text{in}} = 1$  before run 55000 are rejected from **GOLD** and are classified as **BGD**. In the later era, **MCNO** matches the **DATA** more closely for  $D_{\text{Sh-Box}}^{\text{min}} > 200$  cm. It was decided to reject events after run 55000 with  $M_{\text{Shield}}^{\text{in}} = 1$  and  $D_{\text{Sh-Box}}^{\text{min}} < 150$  cm.

This cut still leaves extra **DATA** events, especially for  $150 \text{ cm} < D_{\text{Sh-Box}}^{\text{min}} < 200$  cm, which are due to CR-muons that have fooled all the containment algorithms and which usually appear deep in the detector. Such events are rejected at the check-scan stage, after which the  $D_{\text{Sh-Box}}^{\text{min}}$  distributions for **GOLD** and **MCNO** agree very well (fig. 5.26). This is also true for the distribution of run number, where **MCNO** follows **GOLD** closely (fig. 5.27), giving us confidence that **GOLD** contamination by background is small.

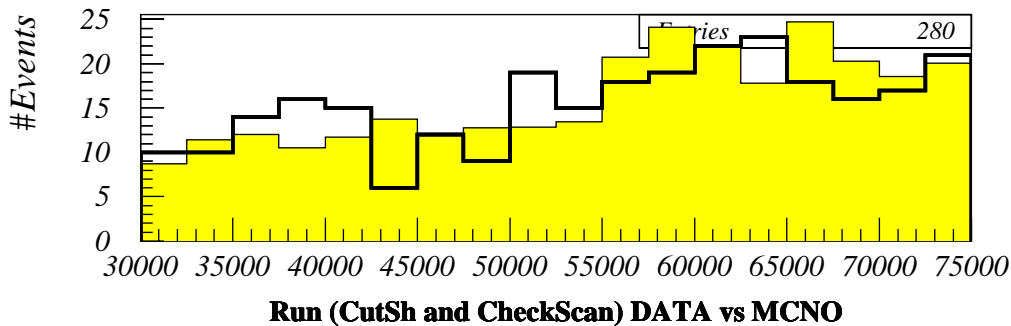
After *CutSh1*, the **GOLD** and **MCNO** acceptances are reduced by 42.6% and 12.3% respectively when all other RINSE cuts (including *CutSh2*) have previously been applied.



• **Figure 5.26:** *CutSh1*. Distributions of  $D_{\text{Sh-Box}}^{\text{min}}$  when  $M_{\text{Shield}}^{\text{in}} = 1$  for **GOLD** (thick line) and **MCNO** normalised to the data exposure by 1/116 (shaded area). All RINSE cuts, including both shield cuts and the check-scan, have been applied.

## 5.4 Acceptance of Event Selection

The acceptance for the neutrino signal, as described by **MCNO** for Soudan 2 data for the period between 26 Aug 1991 to 22 Dec 1996 (runs 30000 to 74999), from generation to the



• **Figure 5.27:** *CutSh1*. Distributions of run number for **GOLD** (thick line) and **MCNO** normalised to the data exposure by 1/116 (shaded area). All RINSE cuts, including both shield cuts and the check-scan, have been applied.

final accepted number, is 22.3% (Table 5.7). Before and after August 1994 the acceptance is 18.6% and 25.7% respectively, because of the different treatment of unit shield multiplicity events. These figures do not take into account the 2% loss of acceptance on the final sample due to the check-scan,<sup>13</sup> discussed in §5.3.6. The total exposure of the experiment for the aforementioned period is 3.341 kTonYears, while the fiducial exposure is 2.679 kTonYears.<sup>14</sup> It is customary to quote the latter number which takes into account the effect of the fiducial volume cuts on the “target” detector volume. The loss of acceptance can be attributed to three major factors: (i) the lack of trigger from low-energy neutrino interactions (or neutral currents), simulated by FILTER, (ii) the fiducial volume and crack cuts, applied by RINSE and (iii) the shield cuts, also applied by RINSE.

A summary of the event selection for **GOLD**, **BGD**, **BGD1** and **BGD2** is given in Tables 5.7 to 5.11. Samples **BGD1** and **BGD2** are subsets of **BGD**, defined in the following section on background contamination and are presented here for the sake of completion.

<sup>13</sup> The overall acceptance for the scanning analysis is 27% for quasi-elastic tracks and 27% for quasi-elastic showers [46].

<sup>14</sup> The exposure has been calculated by EXPOSURE3, a program written by Prof. Earl Peterson for Soudan 2.

		Runs 30000-54999	Runs 55000-74999	Total (All runs)
Exposure (KTon-Years)	Total	1.648	1.693	3.341
	Fiducial	1.306	1.373	2.679
Event Selection Stage		Number of MCNO Events		
Interactions Generated		70692	78322	149014
Passed Rel. 23 FILTER		28058	31561	59619
Passed RINSE CEV cuts		13171	20097	33268
Acceptance		18.6%	25.7%	22.3%
Passed all cuts normalised to data exposure (1/115.7)		113.8	173.7	287.5

• **Table 5.7:** Summary of MCNO event selection divided into early and later eras. The total and fiducial exposures are given at the top. The number of events generated and passing different selection stages is given below. Note there is no check-scan for MCNO.

GOLD	Runs 30000-54999	Runs 55000-74999	Total (All runs)
Event Selection Stage	Number of GOLD Events		
Passed Rel. 23 FILTER + Cut0	2384	1610	3994
Passed RINSE CEV cuts	201	208	409
Passed Check-Scan	126	154	280

• **Table 5.8:** Summary of GOLD event selection divided into early and later eras.

BGD	Runs 30000-54999	Runs 55000-74999	Total (All runs)
Event Selection Stage	Number of BGD Events		
Passed FILTER23 + Cut0	9622	8108	17730
Passed RINSE CEV cuts	834	671	1505
Passed Check-Scan	465	391	856

• **Table 5.9:** Summary of BGD event selection divided into early and later eras.

BGD1	Runs 30000-54999	Runs 55000-74999	Total (All runs)
Event Selection Stage	Number of BGD1 Events		
Passed <b>FILTER23 + Cut0</b>	3660	1835	5495
Passed <b>RINSE CEV cuts</b>	194	105	299
Passed <b>Check-Scan</b>	69	31	100

• **Table 5.10:** Summary of **BGD1** event selection divided into early and later eras.

BGD2	Runs 30000-54999	Runs 55000-74999	Total (All runs)
Event Selection Stage	Number of BGD2 Events		
Passed <b>FILTER23 + Cut0</b>	138	96	234
Passed <b>RINSE CEV cuts</b>	37	28	65
Passed <b>Check-Scan</b>	33	24	57

• **Table 5.11:** Summary of **BGD2** event selection divided into early and later eras.

## 5.5 Comparison to the GOLD Scanned Sample

It is interesting to compare the contained event samples of the fully scanned analysis and of RINSE. The two approaches are very different but reach to comparable event samples. Out of the 280 RINSE **GOLD** events, 207 find their way into the *scanned GOLD* sample. Conversely, there are 117 scanned **GOLD** events that were not selected by RINSE. The differences are due to the following reasons:

- RINSE rejects low energy events which are selected by the scanners: the 3D-hit cut in the scanning analysis rejects track events with less than 6 hits and shower events with less than 9 hits (the scanning shower hit cut is higher in order to reduce breakdown contamination). Approximately 60% of the events selected by the scanners and rejected by RINSE have failed the RINSE 10 3D-hit cut.

- Of the remaining events selected by the scanners and rejected by RINSE, the majority fail the RINSE fiducial volume cut. This occurs because these events have 3D hits in the event box which are outside the fiducial volume. Scanners have chosen to neglect these hits by judging them either (i) as irrelevant to the event or (ii) as part of the event but “clearly” not vetoing it as being outside the fiducial volume – a common example for the latter is 3D hits in the tails of showers, which point from the inside of the detector outwards.
- On the other hand, RINSE accepts events which have one or more prong on cracks and which are rejected by the scanners. It has been demonstrated in this chapter (see Crack Cuts) that these events do not contribute to the background contamination of the **GOLD** sample – they are thus unnecessarily rejected by the scanners.

## 5.6 Background Contamination

In this section the contamination of the **GOLD** sample by non-neutrino interactions is addressed. This exercise is an introduction to background contamination and will be referred to in later chapters.

### 5.6.1 Choice of Background Sample

Three subsets of the **BGD** sample, **BGD1**, **BGD2** and **ROCK**, are introduced here. We are interested in the background sample which best represents the set of physical processes that lead to the contamination of **GOLD** (as described in §5.1, the **BGD** sample). The definitions of the three subsets and the motivation for their study is presented below.

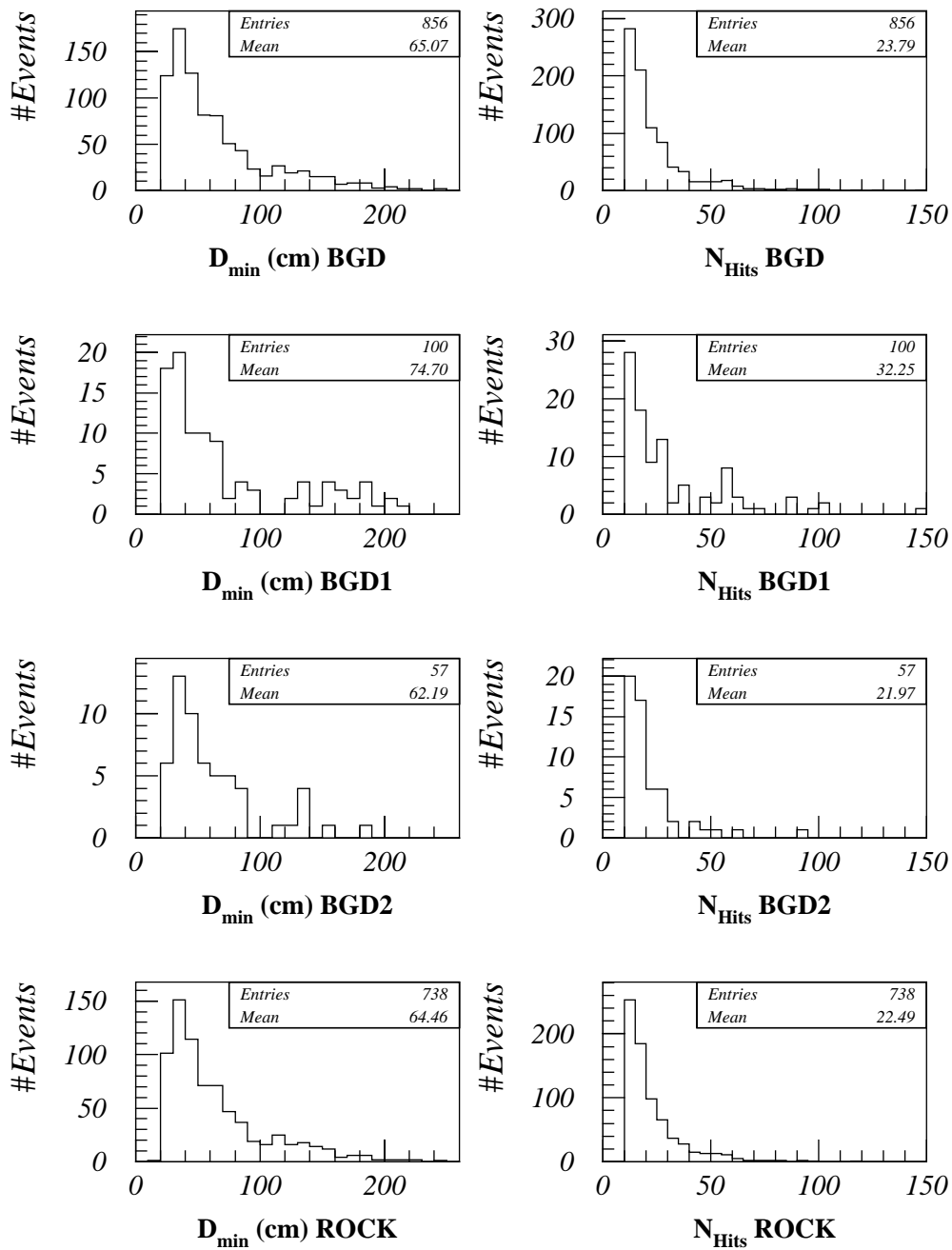
- Events in the **BGD1** sample would have passed the shield cuts but for one shield hit vetoing the event. The **BGD1** sample is enriched in cosmic ray muons entering

the main detector through inter-modular gaps and would be more useful in studying contamination due to shield inefficiency alone.

- Events in the **BGD2** sample have two shield hits which trace a trajectory that does not cross the main detector (TASSO shield counters sitting right on top of the main detector are not considered here), alluding to a charged particle (possibly a CR-muon). The **BGD2** sample is expected to be rich in background events due to neutral particles contaminating the **GOLD** sample. It is worth pointing out that 87.7% of the **BGD2** events passed the check-scan, a percentage even higher than that for **GOLD**. However, its normalisation relative to the **GOLD** sample is unknown so one only hopes to acquire a qualitative understanding of the nature of background. Moreover, the statistics of **BGD2** are scarce.
- Events in the **ROCK** sample have shield multiplicity in the  $T_0$ -window of 2 or above. This background sample is expected to be minimally contaminated by genuine neutrino interactions, because the shield double-coincidence random rate is very small (from **MCNO** it is measured below 2% - fig. 5.21). The population of **ROCK** is 738 events, only 14% lower than that of the parent **BGD** sample.

The complete **BGD** sample is also suited to the background study of **GOLD**. It may be argued, however, that **BGD** contains classes of events, such as those with very high shield multiplicity, which, under no circumstances, may be classified as **GOLD**. Such claims are hard to justify because we have no detailed understanding or simulation of the processes leading to the contamination of **GOLD** by interactions of neutral particles originating in the rock. **BGD** has the higher statistics here.

In practice there is little difference between the four background samples. Their depth ( $D_{\min}$ ) and hit ( $N_{\text{Hits}}$ ) distributions, where  $D_{\min}$  is the minimum distance between any of the event box's eight corners and any of the detector's six faces and  $N_{\text{Hits}}$  is the number of 3D hits in the event box, are remarkably similar (fig. 5.28).



• **Figure 5.28:** Distributions of  $D_{\min}$  (in cm) and  $N_{\text{Hits}}$  for **BGD** (top), and its subsets, **BGD1** (2<sup>nd</sup> from top), **BGD2** (3<sup>rd</sup> from top) and **ROCK** (bottom).

From the depth distributions, the majority of the events are concentrated near the detector's edge. This is expected, since the interaction length of a neutron in the Soudan 2 detector is approx. 80 cm. A small number of events are situated right at the heart of the detector and their nature is harder to understand. They may be due to neutrons that enter the main detector volume through a crack and then scatter and interact inside a module. Such events are typically small – this is also a phase space requirement, since, had they been larger, they would be nearer the outside of the detector.

Most of the background events are small (below 40 hits). This is due to the typically low energy of the neutral particles produced in the rock. Still, some spectacularly large events (above 100 hits) are observed.

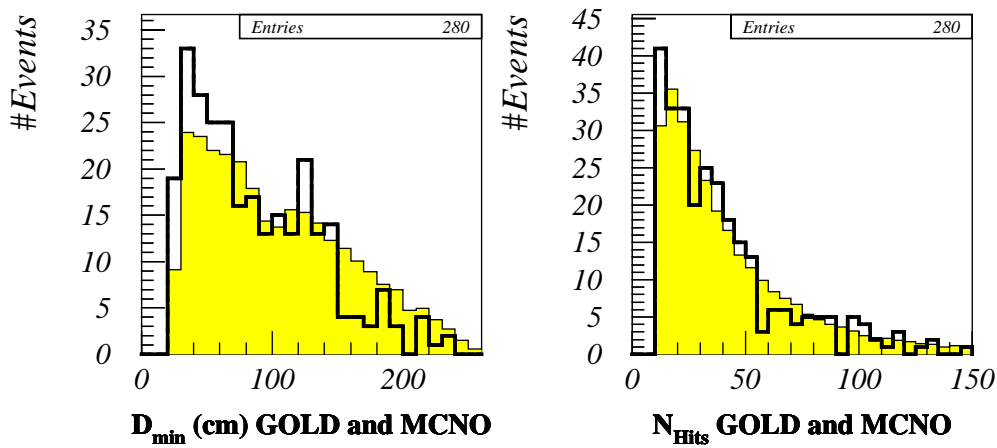
Considering the above, **ROCK** is the event sample chosen to represent the background contamination of **GOLD** for the following reasons:

- It is similar in essence to the other three background samples.
- It has minimal contamination by neutrino events.
- It has high statistics.

### 5.6.2 Depth and Hit Distributions of DATA and MCNO

The contamination of **GOLD** by non-neutrino interactions is prominent in the distributions of  $D_{\min}$  for **GOLD** and **MCNO**, where the latter is normalised to the experiment's exposure (fig. 5.29). The two samples qualitatively agree for  $D_{\min} > 70$  cm but below 70 cm **GOLD** presents considerable excess relative to **MCNO**. On the other hand, the  $N_{\text{Hits}}$  distributions for **GOLD** and **MCNO** agree well, at least on a qualitative level.

It is interesting to examine the correlation between  $D_{\min}$  and  $N_{\text{Hits}}$ . This is presented at fig. 5.30. The  $D_{\min}$  versus  $N_{\text{Hits}}$  space has been divided into six zones, as defined in fig. 5.30. Small events lying near the outside of the detector populate zones 1 and 2, while events deep inside the detector lie in zones 3 and 4. Events near the outside of the



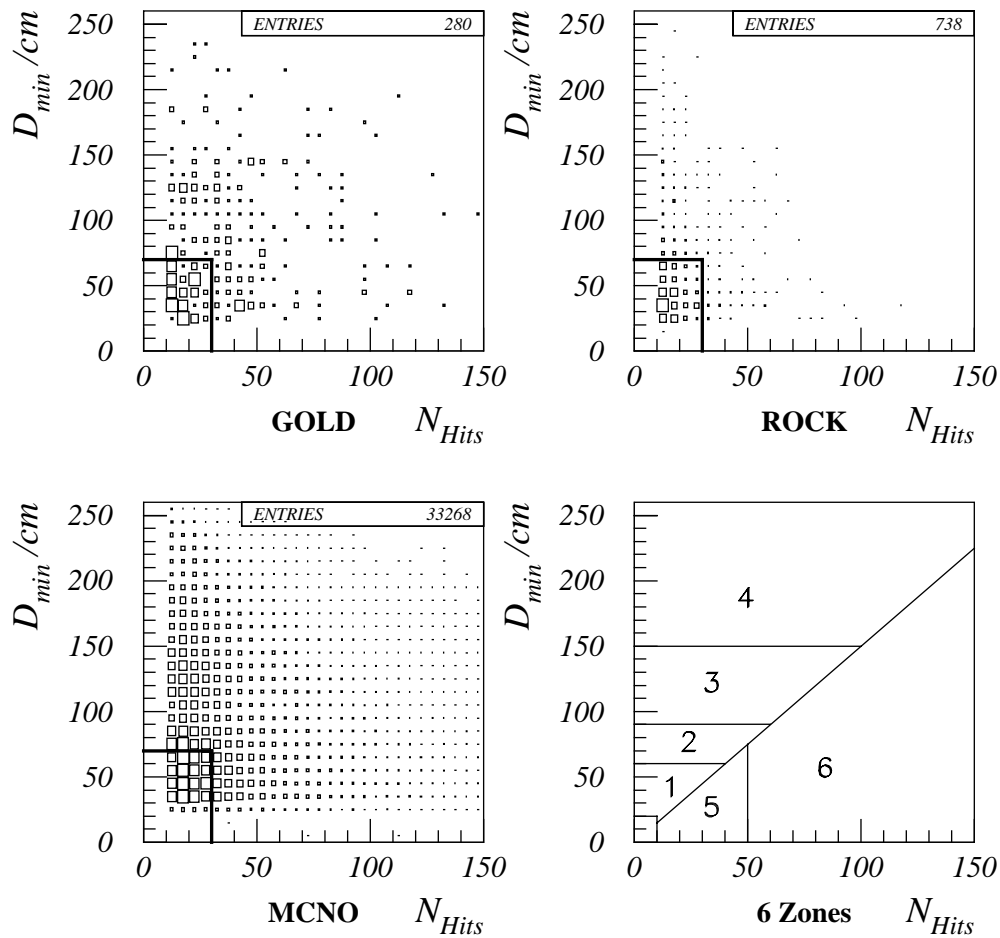
• **Figure 5.29:** Distributions of  $D_{\min}$  (in cm, left) versus  $N_{\text{Hits}}$  (right) for **GOLD** (thick line) and **MCNO** normalised to the experiment's exposure by 1/116 (shaded area).

detector are found in zones 5 and 6. It is worth pointing out that the larger an event is, the closer to the outside it will be (the maximum distance to the outside is  $\approx 260$  cm). The population of each zone for each of the three samples has been recorded in Table 5.12 and graphically represented in fig. 5.31. Unlike **GOLD** and **MCNO**, **ROCK** events are concentrated at low values of  $D_{\min}$  and  $N_{\text{Hits}}$ .

### 5.6.3 A Background Calculation: Fitting to GOLD

The aim of the following fit is to determine the number of neutrinos in the **GOLD** event sample. **GOLD** is described as the sum of some neutrino signal, described by **MCNO**, and some background signal, described by **ROCK**. The neutrino and background signals are not correlated and should be allowed to fluctuate independently.

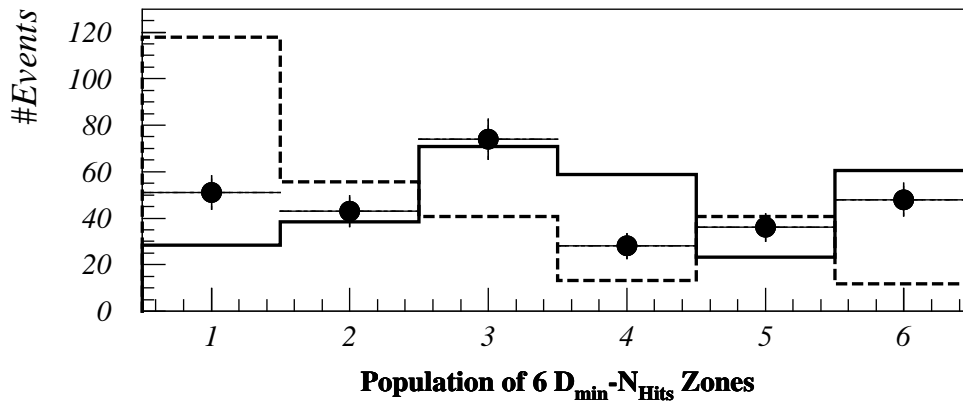
Consider the distributions described in Table 5.12 and fig. 5.31, for **GOLD**, **MCNO** and **ROCK**:  $G_i$ ,  $M_i$  and  $R_i$  respectively, where  $i = 1 \dots n$  and  $n$  is the number of bins of each distribution. The total number of events in each distribution  $G_i$ ,  $M_i$  and  $B_i$  is  $N_G$ ,  $N_M$  and  $N_R$  respectively, which are summarised in Table 5.12. From the above, the **GOLD** distribution,  $G_i$ , may be fitted by the following function:



• **Figure 5.30:** Scatter (box) plots of  $D_{min}$  (in cm) versus  $N_{Hits}$  for **GOLD**, **ROCK** and **MCNO**. The population of each bin is proportional to its side and not its area. The box defines the area of the background reduction cut. The bottom right plot defines the six zones into which the  $D_{min}$  versus  $N_{Hits}$  surface is divided.

Zone	Number of events in each Zone		
	GOLD	MCNO	ROCK
1	51	3362	311
2	43	4554	147
3	74	8430	107
4	28	6971	35
5	36	2761	107
6	48	7190	31
<b>Total</b>	280	33268	738

• **Table 5.12:** Population of each zone of the  $D_{\min}$  versus  $N_{\text{Hits}}$  plot, as defined in fig. 5.30, for GOLD, MCNO and ROCK.



• **Figure 5.31:** Graphic representation of the population of the six zones of  $D_{\min}$  versus  $N_{\text{Hits}}$  space for GOLD (error bars), MCNO (solid line, normalised to GOLD) and ROCK (dashed line, normalised to GOLD).

$$f_i = AM_i + XR_i \quad (5.1)$$

which can be re-written as:

$$f_i = a \frac{N_G}{N_M} M_i + x \frac{N_G}{N_R} R_i \quad (5.2)$$

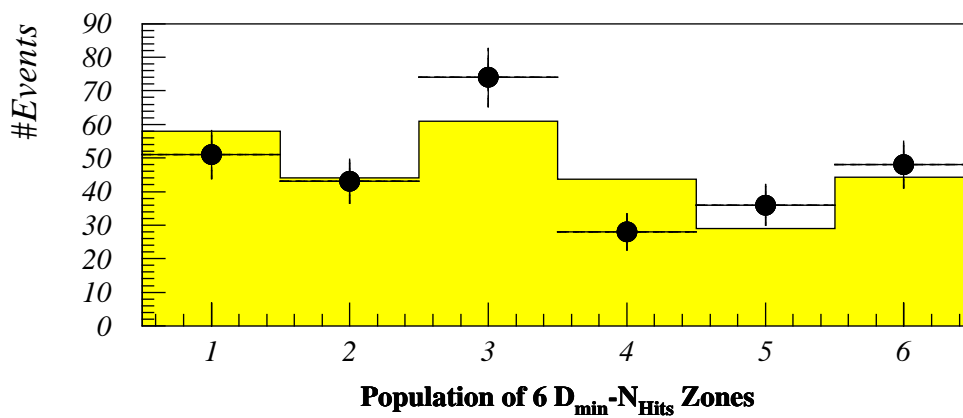
where  $a = AN_M/N_G$  and  $x = XN_R/N_G$ . The fit parameters  $a$  and  $x$  represent the fractions of **GOLD** described by **MCNO** and **ROCK** respectively.

A simple fit will only take into account the fluctuations of  $G_i$  and the goodness of the fit into the error calculation. However, the **ROCK** distribution has finite statistics and its fluctuations must also be included in the final errors. This is also true for **MCNO** but to a much lesser extent, because of its very large population. The method of the ‘‘binned likelihood fit’’ will be implemented, as described in [54] and [74]. The HBOOK routine HMCMLL returns the fractions  $a$  and  $x$  when the distributions  $G_i$ ,  $M_i$  and  $R_i$  are given. They should sum to unity but are not constrained to do so; this is a property of the maximum likelihood approach adopted here.

The results of the fit are summarised in Table 5.13 and fig. 5.32. Approximately one third of the final **GOLD** sample is attributed to non-neutrino events. It is observed that the best fit **ROCK** plus **MCNO** model is not in good agreement with **GOLD** in zones 3 and 4, i.e. for small and medium sized events in the heart of the detector. This could be an indication that the **ROCK** sample is not a good representation of the background contamination in **GOLD**. Alternatively, this may be an indication that the physics model (no oscillations regime) is unsuitable to describe the data. Further discussion is beyond the scope of this chapter. The subject will be revisited in the flavour analysis of the data in chapter 7.

$a$	$0.668 \pm 0.075$
$x$	$0.332 \pm 0.068$
Number of Neutrinos in GOLD = $280 \times a$	$187.0 \pm 21.0$
Number of Background in GOLD = $280 \times x$	$93.0 \pm 19.0$

• **Table 5.13:** Results of background fit in GOLD.



• **Figure 5.32:** Graphic representation of the population of the six zones of  $D_{\min}$  versus  $N_{\text{Hits}}$  space for GOLD (error bars) and the best fit of MCNO plus ROCK (shaded, normalised to GOLD).

### 5.6.4 Effect of Depth and Hit Cuts on Background sample

The background population is clustered at low values of  $D_{\min}$  and  $N_{\text{Hits}}$ . The effect on the populations of the event samples when a background reduction cut, defined by  $D_{\min} > 70 \text{ cm}$  or  $N_{\text{Hits}} > 30$ , is applied is shown in Table 5.15. The **ROCK** acceptance is reduced by 58%, while that of **MCNO** has only dropped by 14%. The **GOLD** acceptance is affected more than that of **MCNO**, an indication in favour of the hypothesis that **GOLD** is contaminated by background.

A harsher cut may be applied, rejecting all events below 40 hits. The outcome is presented in Table 5.14. Now only 10% of **ROCK** survives the cut. The background contamination in **GOLD** is estimated to be less than 10%, assuming **ROCK** to be a good model for the background. The large events sample will be an interesting set to look for new Physics effects in an almost background-free environment.

Number of events	<b>GOLD</b>	<b>MCNO</b>	<b>ROCK</b>	<b>BGD</b>
<b>Final sample (N)</b>	280	33268	738	856
<b>After CutBGD (<math>N^{\text{Pass}}</math>)</b>	208	28533	308	370
<b>Fraction (T) passing CutBGD</b>	$0.743 \pm 0.026$	$0.858 \pm 0.002$	$0.417 \pm 0.017$	$0.432 \pm 0.017$

• **Table 5.15:** Number and fraction of events passing the BGD-cut for **GOLD**, **MCNO**, **ROCK** and **BGD**. The error on T is given by  $\sqrt{T(1-T)/N}$ , since N and  $N^{\text{Pass}}$  are correlated.

Number of events	<b>GOLD</b>	<b>MCNO</b>	<b>ROCK</b>	<b>BGD</b>
<b>Final sample (N)</b>	280	33268	738	856
<b>After 40+ Hit Cut (<math>N^{\text{Pass}}</math>)</b>	105	13899	72	97
<b>Fraction (T) passing Hit cut</b>	$0.375 \pm 0.029$	$0.412 \pm 0.003$	$0.098 \pm 0.011$	$0.113 \pm 0.011$

• **Table 5.14:** Number and fraction of events passing the 40+ hit cut for **GOLD**, **MCNO**, **ROCK** and **BGD**. The error on T is given by  $\sqrt{T(1-T)/N}$ , since N and  $N^{\text{Pass}}$  are correlated.